



## Co-processing of fossil feedstock with lignin-derived model compound isoeugenol over Fe-Ni/H-Y-5.1 catalysts



Zuzana Vajglová<sup>a</sup>, Bibesh Gauli<sup>a</sup>, Päivi Mäki-Arvela<sup>a</sup>, Irina L. Simakova<sup>b</sup>, Narendra Kumar<sup>a</sup>, Kari Eränen<sup>a</sup>, Teija Tirri<sup>a</sup>, Robert Lassfolk<sup>a</sup>, Markus Peurla<sup>c</sup>, Dmitry E. Doronkin<sup>d</sup>, Dmitry Yu. Murzin<sup>a,\*</sup>

<sup>a</sup> Åbo Akademi University, Johan Gadolin Process Chemistry Centre, Henriksgatan 2, 20500 Turku/Åbo, Finland

<sup>b</sup> Borekov Institute of Catalysis, Novosibirsk, Russia

<sup>c</sup> Institute of Biomedicine, University of Turku, Kiinamyllynkatu 10, 20520 Turku, Finland

<sup>d</sup> Institute of Chemical Technology and Polymer Chemistry, and Institute of Catalysis Research and Technology, Karlsruhe Institute of Technology, Kaiserstrasse 12, 76131 Karlsruhe, Germany

### ARTICLE INFO

#### Article history:

Received 21 September 2022

Revised 2 March 2023

Accepted 6 March 2023

Available online 9 March 2023

#### Keywords:

Co-processing

Bio-fuel

Lignin-derivative

Fe-Ni catalysts

Hydrodeoxygenation

Isoeugenol

Hexadecane

### ABSTRACT

Co-processing of n-hexadecane with lignin derived isoeugenol as a model compound was investigated in this work using low-cost mono- and bimetallic iron and nickel supported on H-Y-5.1 zeolite. Different Fe-Ni metal ratios in the catalyst led to different reaction rates of processes and product distribution. The presence of just 0.26 wt% isoeugenol in the mixture with n-hexadecane made hydroisomerization-hydro cracking of the latter two-fold less active. Catalysts with smaller metal particle sizes, lower than 6 nm were more efficient pointing out on structure sensitivity. Extremely high activity in co-processing was obtained over 2 wt% Fe – 8 wt% Ni/H-Y-5.1 catalysts with the median metal particle size of 4.6 nm and metals-to-acid site ratio of 8.6. Fe catalyst were much less active in isoeugenol hydrodeoxygenation, while high cracking activity of hexadecane was observed in the presence of Ni. Alkylation of n-hexadecane was a feature of 8 wt% Fe – 2 wt% Ni/H-Y-5.1, whereas, over the 5 wt% Fe – 5 wt% Ni/H-Y-5.1 bifunctional catalyst no undesired oxygen-containing cyclic products were detected. This catalyst exhibited the highest hydrogen consumption according to temperature programmed desorption, which can serve as a marker for efficient hydrodeoxygenation. The spent catalysts contained ca 40 wt% of coke with predominantly aliphatic species.

© 2023 The Author(s). Published by Elsevier Inc. This is an open access article under the CC BY license (<http://creativecommons.org/licenses/by/4.0/>).

## 1. Introduction

Due to depletion of fossil-based feedstock and environmental concerns associated with fossil fuels, lignocellulosic biomass has sparked substantial attention as a source of renewable liquid fuels and chemicals [1–3]. For decades, lignocellulosic biomass has been utilized in the Kraft process. The primary components of biomass, such as hemicellulose and lignin, are burned as a low-value fuel in this process, whereas cellulose is used to manufacture pulp. Due to its distinctive structure, lignin, which is currently underutilized, offers immense potential as a source of renewable fuels, chemicals, and aromatic compounds. Because lignin has a lower oxygen-to-carbon atomic ratio compared to carbohydrates, its derivatives could be used as fuel [2–8].

Fast pyrolysis and flash pyrolysis to convert lignocellulosic biomass to liquid fuels is often considered as a cost-effective method

for biomass conversion requiring lower temperatures compared to e.g. gasification. Fe modified and acidic H-Y, H-Beta and H-Ferrierite microporous zeolite catalysts have been used for upgrading lignocellulosic biomass pyrolysis vapours to value added fuels and chemicals in a fluidized bed reactor [9]. In the fast pyrolysis process, biomass is thermally degraded in the absence of oxygen at a moderate temperature ranging between 723 and 873 K with a residence time of less than two seconds. Through this procedure, the yield of condensed bio-oil including such compounds as aldehydes, ketones, alcohols, phenolics, and other phenolic compounds can reach up to 75%. In particular, guaiacol (ca. 39%), phenol, anisole, cresol, syringol, and others are produced via lignin fast pyrolysis. Additionally, char, noncondensable gases such as carbon dioxide and methane, and water are also formed [2,10,11].

However, this bio-oil, as such, is unsuitable for the use as a liquid transportation fuel [12,13] due to low pH, instability as well as high O content and mediocre calorific value. A feasible technique for upgrading pyrolysis bio-oil pyrolysis for fuel

\* Corresponding author.

E-mail address: [dmurzin@abo.fi](mailto:dmurzin@abo.fi) (D.Yu. Murzin).

production could be hydrodeoxygenation (HDO). In this reaction, oxygen-containing compounds are transformed to oxygen-free hydrocarbons and water in the presence of a catalyst at ca. 573 K and a high pressure of H<sub>2</sub> (up to 20 MPa) [2,14]. Catalytic HDO reactions are often catalyzed by noble metals, transition metal carbides, bifunctional metals, and metal sulfides supported on metal oxides or carbon [4,15–19]. During catalytic HDO a variety of reactions occurs, including decarboxylation, hydrogenation, hydrocracking, hydrogenolysis, and dehydration, modifying the C–O–C, C–O–H, and C–C links [4]. Because lignin-derived phenols contain a variety of functional groups such as alkyl, hydroxyl, alkoxy, olefinic double bonds, etc., there is a competition between HDO processes and double bond/aromatic ring hydrogenation reactions during upgrading of these compounds. Excessive ring hydrogenation is undesirable because of a significant hydrogen consumption in such reactions.

Transformations of pyrolysis oils are challenging to understand and model because of many reactions are occurring at the same time. Therefore, several lignin-derived bio-oil model compounds have been widely studied in the literature to understand the reaction pathways and the corresponding mechanism. Guaiacol [20–23] was often the preferred prototype chemical to represent lignin-derived bio-oils. Similarly, other lignin-derived oxygenates have been described in the literature as model compounds, namely phenol [21,24,25], cresol [21,26,27], anisole [21,28,29], vanillin [30–32], eugenol [33–37], isoeugenol [12,26,38–40] reflecting their similarities with the depolymerized lignin.

Several attempts have been made recently to promote the use of renewable energy and limit green-house gas emissions including energy and climate targets facilitating energy security to promote decarbonized economy and the use of biofuels of specific action plans have been established [41]. One step forward to reach these targets is to utilize the existing infrastructure of the petroleum refineries via co-processing of renewable feedstock with fossil ones [42,43]. Co-processing of bio-oils in fluid catalytic cracking has been intensively studied, however, several challenges have been identified due to a high water content in bio-oil [44]. In order to understand the interactions between oxygenated and fossil feedstock during co-processing, also model compounds have been used [45], such as phenol, syringol, trimethoxybenzene with tetralin and benzene. Moreover, straight run gas oil (SRGO) has been co-processed with e.g. guaiacol and anisole over CoMo/ $\gamma$ -Al<sub>2</sub>O<sub>3</sub> catalyst in a fixed bed reactor [46]. SRGO was also co-processed with different fractions of pyrolysis oil over Ru/C catalyst [47]. Interestingly a competition between hydrodeoxygenation and hydrodesulfurization (HDS) steps when feeding oxygenated phenolic compounds with SRGO was observed, which was not, however, permanent, because with a neat SRGO feed HDS activity was recovered.

In the current work, hexadecane and isoeugenol were selected as a fossil and lignin derived model compounds, respectively. Hexadecane represents a model compound for hydrocracking and isoeugenol for hydrodeoxygenation. It should be pointed out here, that hexadecane can also originate from renewable sources, for example from non-edible oils [48], when it is not competing with the food chain. Hydrodeoxygenation of palmitic acid for production of hexadecane has been demonstrated over MoO<sub>2</sub>/CNT catalyst [49]. In addition, hexadecane hydrocracking has been successfully demonstrated over several Ru-, and Ni catalysts for production of jet fuels [50–52]. The reaction network of n-hexadecane hydroisomerization-hydrocracking over bifunctional metal–acid catalysts [50,51,53,54] is shown in Fig. 1.

Isoeugenol was selected as a representative lignin-derived bio-oil model phenolic compound of oxygenated groups due to its molecular structure consisting of methoxy, hydroxy, and allyl groups in the aromatic ring [26]. Isoeugenol is present in wood

sawdust as a waste residue from oak and pine wood and, at the same time, hydrodeoxygenation of isoeugenol has been less intensively studied compared to other phenolic compounds. The reaction network of isoeugenol hydrodeoxygenation with potential side reactions based on the previous studies with Ni-, Co-, Pt-, Ir-, Re-supported catalysts [12,26,38,40] is shown in Fig. 2.

At 473 K and 3 MPa hydrogen, Bomont et al. [38] demonstrated that HDO of isoeugenol occurs promptly and completely, giving a high yield of the desired propylcyclohexane over Pt/H-Beta zeolites. At 523 K and 3–4 MPa hydrogen pressure, similar results were obtained in [40,55] over bimetallic Pt-Re and Ir-Re catalysts on alumina, a support bearing Lewis acidity. Disadvantages of these catalysts are the high prices of noble metals [4,19]. In Ni, Co catalysts [12], no direct effect of the support material (zeolites, SiO<sub>2</sub>, Al<sub>2</sub>O<sub>3</sub>, TiO<sub>2</sub>) on isoeugenol hydrodeoxygenation was observed. As a result, in the recent years, the research has mainly concentrated on the iron triad (Fe, Co, Ni) based catalysts as a less expensive option of the HDO process. Generally Fe-based catalysts show high activity in selective cleavage of C–OH, C–O bonds while exhibiting low activity in the ring hydrogenation. On the other hand, Co- and Ni-based catalysts demonstrated high activity in dihydrogen dissociation, and hydrogenation [12,26]. Therefore, the bimetallic systems comprising Fe and Ni are potentially promising catalysts for co-processing.

The current work is focusing on the synergistic effect of Fe-Ni metals in the co-processing of hexadecane with isoeugenol. For this purpose, the monometallic catalysts and the bimetallic catalysts with a varied ratio between Fe and Ni were used with H-Y-5.1 zeolite as a support. The use of Ni-Fe is also encouraged by the recent studies demonstrating hydrodeoxygenation of waste cooking oil [56] and hydrocracking of coconut oil [57] over supported Ni-Fe catalysts. Taking into account that phenolic compounds are typically adsorbed stronger because of the aromatic ring, the straight chain alkane was used in a large excess.

## 2. Experimental

### 2.1. Preparation and characterization of the fresh catalysts

To study the influence of the metal on the co-processing of n-hexadecane with lignin derived isoeugenol, a series of Fe, Ni, and Fe-Ni supported bifunctional catalysts on a commercial H-Y-5.1 zeolitic support have been prepared (Table 1). All catalysts were synthesized by the incipient wetness impregnation with an aqueous solution of the corresponding nitrate precursor, Fe(NO<sub>3</sub>)<sub>3</sub>·9H<sub>2</sub>O (Sigma-Aldrich) or Ni(NO<sub>3</sub>)<sub>2</sub>·6H<sub>2</sub>O (CJSC Souzchimprom), respectively. Characterization was made by several physico-chemisorption methods as described below.

Textural properties were determined with nitrogen physisorption (Micromeritics 3Flex-3500) degassing the samples first ex situ under vacuum at 473 K for 8 h followed by pre-treatment in the physisorption equipment per se under vacuum for 5 h at 453 K. The specific surface area and the pore size distribution were calculated using the Dubinin-Radushkevich and the non-local density functional theory methods, respectively.

Qualitative and quantitative determination of Brønsted and Lewis acid sites was done using pyridine ( $\geq 99\%$ , Acros Organics) as a probe molecule by Fourier transform infrared spectroscopy (FTIR, ATI Mattson). After pretreatment of a thin self-supporting pellet inside the FTIR cell at 723 K under vacuum and decreasing temperature to 373 K, the background spectra were recorded. Adsorption of pyridine was done for 30 min at 373 K followed by measurements after desorption at various temperatures. The interval between 523 and 623 K reflects all sites, 623–723 K correspond to medium sites, while spectra after desorption at 723 K were

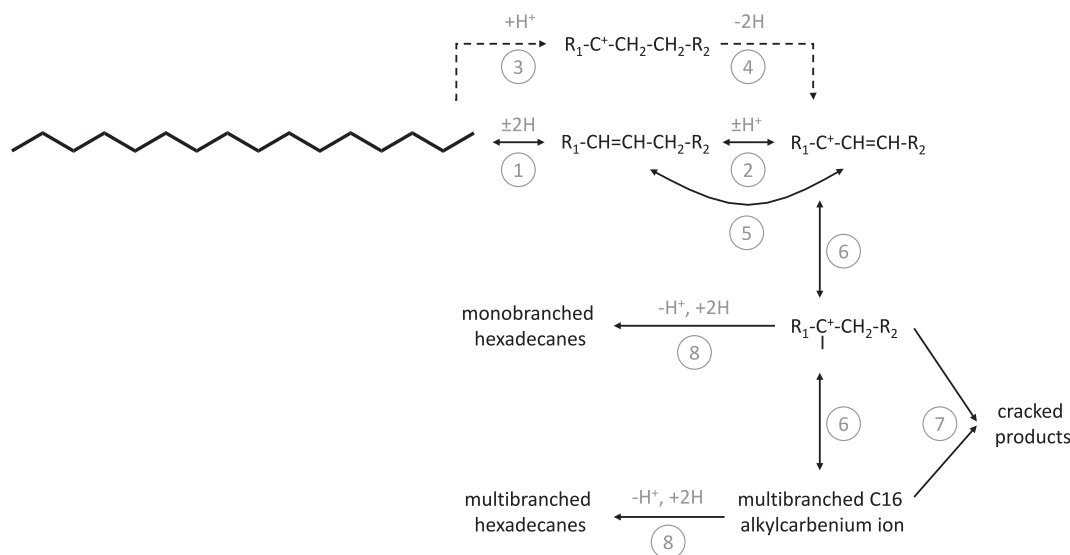


**Fig. 1.** Scheme of n-hexadecane hydroisomerization-hydrocracking. 1 – hydrogenation-dehydrogenation on metallic sites, 2 – protonation-deprotonation on acid sites, 3 – addition of proton to form alkylcarbenium ion on acid, 4 – dehydrogenation to form alkylcarbenium ion, 5 – competitive adsorption–desorption of alkene and carbenium ion on acid sites, 6 – rearrangement of alkylcarbenium ion, 7 – cracking of alkylcarbenium ion, 8 – hydrogenation to form alkane on metallic sites.

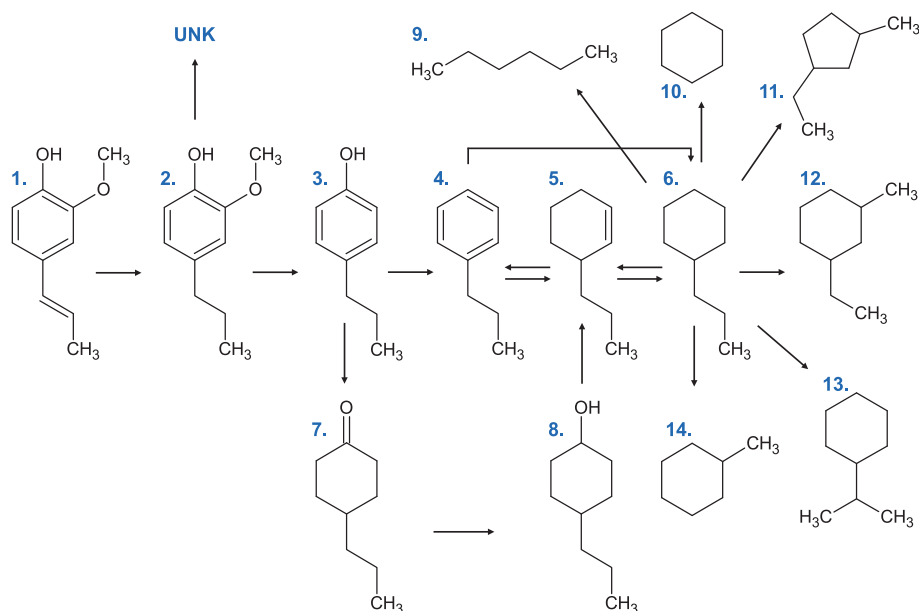


**Fig. 2.** Scheme of isoeugenol hydrodeoxygenation with potential side reaction over Ni-, Co-, Pt-, Ir-, Re-supported catalysts. Legend: isoeugenol (1), dihydroeugenol (2), 4-propylphenol (3), propylbenzene (4), propylcyclohexene (5), propylcyclohexane (6), 4-propylcyclohexanone (7), 4-propylcyclohexanol (8), hexane (9), cyclohexane (10), 1-methyl-3-ethylcyclopentane (11), 1-methyl-3-ethylcyclohexane (12), isopropylcyclohexane (13), methylcyclohexane (14), unknown products, oligomers or strongly adsorbed compounds on the catalyst surface [26] (UNK).

**Table 1**

List of catalysts, nominal loading, and the metal fraction determined by ICP-OES.

Code	Catalyst	Metal fraction, mol%	
		Fe	Ni
Fe <sub>5</sub>	5 wt% Fe/H-Y-5.1	100.0	0.0
Fe <sub>3</sub> Ni <sub>2</sub>	8 wt% Fe – 2 wt% Ni/H-Y-5.1	80.8	19.2
Fe <sub>3</sub> Ni <sub>5</sub>	5 wt% Fe – 5 wt% Ni/H-Y-5.1	51.2	48.8
Fe <sub>2</sub> Ni <sub>8</sub>	2 wt% Fe – 8 wt% Ni/H-Y-5.1	20.8	79.2
Ni <sub>5</sub>	5 wt% Ni/H-Y-5.1	0.0	100.0

attributed to strong sites. Quantification of the Brønsted and Lewis acid sites was based on the spectral bands at 1545 cm<sup>-1</sup> and 1450 cm<sup>-1</sup>.

Concentration of metals in the bulk of the catalyst was performed by inductively coupled plasma – optical emission spectrometry (ICP-OES, PerkinElmer Optima 5300 DV instrument) digesting the catalyst in a mixture of 30% HCl (Sigma-Aldrich), 65% HNO<sub>3</sub> (Sigma-Aldrich) and 50% HBF<sub>4</sub> (Sigma-Aldrich) mixture.

The phase purity and identification of the crystal phases was performed by powder X-ray diffraction (XRD) for pre-reduced ex-situ catalysts using D8 Advance diffractometer (Bruker, Germany) with Bragg-Brentano geometry, CuKα radiation ( $\lambda = 1.5418 \text{ \AA}$ ) and a one-dimensional LynxEye detector. The 2θ-angle was scanned from 15° to 70° with 0.05° step.

Jeol JEM-1400Plus with 120 kV acceleration voltage and 0.38 nm resolution and an Osis Quemesa 11 Mpix

bottom-mounted digital camera were utilized to investigate the metal particle size.

Zeiss Leo Gemini 1530 Scanning Electron Microscope with a Thermo Scientific UltraDry Silicon Drift Detector (SDD) was applied for scanning electron microscopy (SEM).

The  $^{29}\text{Si}$  and  $^{27}\text{Al}$  MAS NMR spectra was recorded on a Bruker AVANCE-III spectrometer operating at 79.50 MHz ( $^{29}\text{Si}$ ) and 104.26 MHz ( $^{27}\text{Al}$ ) equipped with a CP-MAS 4 mm solid state probe. The  $^{27}\text{Al}$  spectra were recorded using a 5.00  $\mu\text{s}$  pulse and a recycle delay of 0.05 s at 14 kHz spinning speed. The  $^{29}\text{Si}$  spectra were recorded using a 3.84  $\mu\text{s}$  pulse and a recycle delay of 100 s at 14 kHz spinning speed.

The spectra of  $^{57}\text{Fe}$  Mössbauer spectroscopy in the transmission geometry were recorded at 295 K with a 18-month-old  $^{57}\text{Co}$ :Rh source (Ritverc Co. 50 mCi June 2020) with a maximum Doppler velocity of 11.0 mm/s.

For temperature programmed reduction Microtrac Belcat II equipment was used pre-treating a catalyst sample at 473 K for 2 h in argon followed by cooling to 323 K and subsequent heating under 5 vol%  $\text{H}_2$  and 95 vol% Ar flow to 1073 K with a 5 K/min ramp.

X-ray absorption spectroscopy was used to probe the bulk-averaged element specific local structure around Fe and Ni atoms. XAS spectra at Fe and Ni K absorption edges were recorded at the P65 beamline of PETRA III synchrotron radiation source (DESY, Hamburg) in transmission mode for calcined and reduced bimetallic catalysts. The  $k^2$ -weighted EXAFS functions were Fourier transformed (FT) in the  $k$  range of 2–14  $\text{\AA}^{-1}$  and multiplied by a Hanning window with a sill size of 1  $\text{\AA}^{-1}$ .

## 2.2. Catalytic tests

The catalytic experiments of co-processing were carried out in a batch reactor (PARR instruments, 300 mL). Isoeugenol (98%, mixture of *cis* and *trans*, Sigma-Aldrich) and *n*-hexadecane ( $\geq 99\%$ , Alfa Aesar) were employed as the reactants. Based on the corresponding TPR profiles, the catalyst was activated in the flow of hydrogen (40 mL/min) in a two-step reduction procedure: 298–523 K (hold 2 h) and 523–773 K (hold 2 h) with the temperature ramp of 2  $^\circ\text{C}/\text{min}$ .

The catalyst screening experiments were performed at 573 K for 4 h and 3 MPa of  $\text{H}_2$  (99.999%, AGA) with 100 mL of hexadecane, 200 mg of isoeugenol and 100 mg of the catalyst. The catalyst sieved fraction was below 63  $\mu\text{m}$  to eliminate internal mass-transfer limitations and the mechanical stirrer of the reactor operated at 1000 rpm to overcome external mass-transfer limitations.

At regular time intervals, the liquid samples were collected and analyzed using a gas chromatograph (GC, Agilent 6890 N) with DB-1 column (30 m  $\times$  250  $\mu\text{m}$   $\times$  0.5  $\mu\text{m}$ ). Temperature of the FID detector was 553 K. The temperature program was: 333 K for 5 min, then heating to 408 K with a temperature ramp of 3 K/min, followed by holding for 1 min and ramping to 573 K with 15 K/min. The following chemicals were used for calibration: isoeugenol (98%, mixture of *cis* and *trans*, Sigma-Aldrich), dihydroeugenol ( $\geq 99\%$ , Sigma-Aldrich), propylcyclohexane (99%, Sigma-Aldrich), hexane ( $\geq 99\%$ , Fluka), heptane ( $\geq 99\%$ , Sigma-Aldrich), octane ( $\geq 99\%$ , Merck), nonane ( $\geq 99\%$ , Sigma-Aldrich), decane ( $\geq 99.5\%$ , Sigma-Aldrich), cyclohexane ( $\geq 99.9\%$ , Alfa Aesar), 2,5-dimethylhexane (99%, Sigma-Aldrich), ethylbenzene ( $\geq 99.5\%$ , Merck). The same column and the same temperature program were used for the GC-MS analysis (Agilent GC/MS 6890N/5973) to confirm other products.

The calibration constants for non-calibrated *n*-alkanes, C3–C18, was calculated based on the calibrated *n*-alkanes, C6–C10, and relative response factors of *n*-alkanes = 0.171  $\times$  carbon number – 0.405 reported in [58] for Zebron ZB-5 fused silica cap-

illary column (30 m  $\times$  0.25 mm  $\times$  0.25  $\mu\text{m}$ ). The linear response factors of *n*-alkanes with the comparable slope of 0.188 was reported in [59] for HP-5 (0.25 mm  $\times$  30 m  $\times$  0.25 mm) capillary column.

## 2.3. Characterization of the spent catalysts

Thermogravimetric analysis (TGA) was used to determine coke on the spent catalyst using SDT650 instrument (TA Instruments). In air flow of 100 mL/min, ca 5 mg of catalyst, loaded into 90  $\mu\text{L}$  alumina cup, was heated up to 800  $^\circ\text{C}$  (held 5 min) with the heating ramp 10  $^\circ\text{C}/\text{min}$ . Results obtained for the spent catalyst were compared to the results for the fresh one.

The soluble hydrocarbons trapped in the spent catalyst (coke) have been identified based on the often used procedure, namely, a soluble coke extraction with  $\text{CH}_2\text{Cl}_2$  [60–62], introduced by Guisnet et al. [63]. Approximately, 20 mg of the spent catalyst in the polyethylene vial was dissolved in 2 mL of 40% HF (Merck KGaA) for 5 h at ambient temperature and for 2 h in an ultrasonic bath. In the second step, a solution was neutralized by ca. 30 mL of 1 M solution of NaOH. Finally, the organics were extracted overnight by adding 1 mL of dichloromethane ( $\text{CH}_2\text{Cl}_2 \geq 99.9\%$ , GC, Sigma-Aldrich). Extracts (organic phase) were analyzed by NMR and GC-MS (Agilent GC/MS 6890N/5973) using the same column and the same temperature program (held for 10 extra minutes) as for the reaction product analysis. Before NMR analysis of the extracted coke, first, dichloromethane was evaporated and as a solvent  $\text{CDCl}_3$  was used.  $^1\text{H}$  NMR analysis in the solution state was performed using a Bruker Avance-III spectrometer operating at 500.20 MHz ( $^1\text{H}$ ) equipped with a Smartprobe: BB/1H was used. The reported signals are referenced to an internal standard (TMS  $\delta\text{H} = 0.0$  ppm).

## 2.4. Definitions

The conversion of isoeugenol ( $X_{\text{IE}}$ ) was calculated by:

$$X_{\text{IE}} = \frac{n_{\text{IE},0} - n_{\text{IE},t}}{n_{\text{IE},0}} * 100\% \quad (1)$$

where  $n_{\text{IE},0}$  is the initial isoeugenol molar concentration and  $n_{\text{IE},t}$  is the isoeugenol molar concentration at time  $t$ .

The conversion of dihydroeugenol ( $X_{\text{DHE}}$ ) was calculated by:

$$X_{\text{DHE}} = \frac{n_{\text{IE},0} - n_{\text{IE},t} - n_{\text{DHE},t}}{n_{\text{IE},0} - n_{\text{IE},t}} * 100\% \quad (2)$$

where  $n_{\text{DHE},t}$  is the dihydroeugenol molar concentration at time  $t$ .

The conversion of *n*-hexadecane ( $X_{\text{HXD}}$ ) was calculated by:

$$X_{\text{HXD}} = \frac{n_{\text{HXD},0} - n_{\text{HXD},t}}{n_{\text{HXD},0}} * 100\% \quad (3)$$

where  $n_{\text{HXD},0}$  is the initial *n*-hexadecane molar concentration and  $n_{\text{HXD},t}$  is the *n*-hexadecane molar concentration at time  $t$ .

Conversion in co-processing ( $X_{\text{IE+HXD}}$ ) was calculated in the following way:

$$X_{\text{IE+HXD}} = X_{\text{IE}} \cdot x_{\text{IE},0} + X_{\text{HXD}} \cdot x_{\text{HXD},0} \quad (4)$$

where  $x_{\text{IE},0}$  is the initial mass fraction of isoeugenol and  $x_{\text{HXD},0}$  is the initial mass fraction of *n*-hexadecane.

The liquid phase mass balance of cyclic compounds (MB) was calculated by:

$$\text{MB} = \frac{\text{MB}_t}{\text{MB}_0} * 100\% \quad (5)$$

where  $\text{MB}_t$  is the sum of liquid-phase reactants and products at time  $t$ , and  $\text{MB}_0$  is the sum of liquid-phase reactants and products at the beginning of the reaction (time 0). The compounds not

included in Eq. (5) are gas-phase products, and heavy compounds adsorbed on the catalyst (coke).

The carbon balance (CB) was calculated by:

$$CB = \frac{\sum n_{i,t} \cdot CN_i}{n_{IE,0} \cdot CN_{IE} + n_{HXD,0} \cdot CN_{HXD}} * 100\% \quad (6)$$

where  $n_{i,t}$  is molar concentration of  $i$  compound at time  $t$ , and  $CN$  is the carbon number.

Yields of products ( $Y_{i,t}$ ) were calculated by:

$$Y_i = \frac{n_{i,t}}{n_{IE,0} + n_{HXD,0}} * 100\% \quad (7)$$

The reaction rates ( $r$ ) and turnover frequency (TOF) per metals and acid sites are calculated as follows:

$$r = \frac{\Delta n}{\Delta t \cdot m_{cat}} \quad (8)$$

$$TOF = \frac{\Delta n}{\Delta t \cdot n_{metals(surface)}} \quad (9)$$

$$TOF^* = \frac{\Delta n}{\Delta t \cdot n_{acid\ sites}} \quad (10)$$

Where  $\Delta n/\Delta t$  denotes reacted moles (e.g. hexadecane or dihydroeugenol) per time interval  $\Delta t$  (one to 30 min) in a batch reactor,  $m_{cat}$  is the catalyst mass. In the calculations of TOF and TOF\* it was considered that both metals are active and different options of acidity were tried (e.g. total, Brønsted, and Lewis acid sites; weak, medium, and strong sites), respectively, where  $n_{metals(surface)} = (n_{(Fe)} \times dispersion_{(Fe)}/100 + n_{(Ni)} \times dispersion_{(Ni)}/100)$  is exposed moles of metals,  $n_{acid\ sites}$  is moles of acid sites.

### 3. Results and discussion

#### 3.1. Catalyst characterization results

Reduction profiles of the catalysts determined by TPR, indicating interactions between iron and nickel for the three fresh catalysts are given in Fig. 3. In the reduced  $Fe_2Ni_8$  and  $Fe_5Ni_5$  catalysts, quasi in situ X-ray absorption spectra showed a tight contact between Fe and Ni with formation of surface Fe-enriched fcc FeNi random alloys. However, the presence of alloy was not clearly confirmed by XRD in the reduced  $Fe_5Ni_5$  catalyst (Fig. S1).

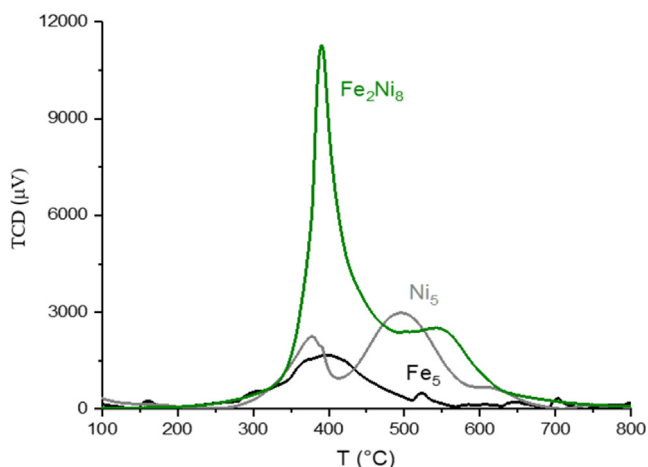


**Fig. 3.**  $H_2$ -TPR profiles of  $Fe_5$  (black),  $Fe_2Ni_8$  (green),  $Ni_5$  (grey). Conditions: to 1073 K with a 5 K/min ramp under 1.5 mL/min of hydrogen and 28.5 mL/min of argon (5 vol%  $H_2$  and 95 vol% Ar). (For interpretation of the references to colour in this figure legend, the reader is referred to the web version of this article.)

**Table 2**

Metal content (determined by ICP-EOS) of different Fe, Ni and Fe-Ni/H-Y-5.1 fresh catalysts, their concentrations of Brønsted and Lewis acid sites determined by pyridine adsorption-desorption, median metal particle sizes of the fresh and spent catalysts determined by TEM, and textural properties of the spent catalysts. Legend: BAS – Brønsted acid sites, LAS – Lewis acid sites, TAS – total acid sites, B/L – ratio of the Brønsted and Lewis acid sites, s (strong acid sites, data at 723 K), m (medium acid sites, data at 623 K minus data at 723 K), and w (weak acid sites, data at 523 K minus data at 623 K).  $C_{Fe-Ni}/C_{TAS}$  – metals-to-total acid site, S – specific surface area, V – total pore volume,  $\Delta$  – difference between fresh and spent catalysts after catalyst screening experiments,  $n_{coke}$  – deposited coke in the spent catalyst determined by TGA.

Catalyst	Metal concentration		BAS		LAS		TAS		B/L	$C_{Fe-Ni}/C_{TAS}$	$d_{FEM, fresh}$	$d_{FEM, spent}$	$S_{spent}$	$V_{spent}$	$\Delta S$	$\Delta V$	$n_{coke}$
	Fe	Ni	w	s	w	s	$\Sigma$	$\Sigma$									
$Fe_5$	4.47	0	106	194	6	0	12	313	25	2.6	5.4	5.5	9	0.03	-98	-85	n.a.
$Fe_8Ni_2$	7.15	1.82	53	60	113	46	47	160	2.4	9.9	6.3	8.3	350	0.16	-45	-47	35
$Fe_5Ni_5$	4.37	4.4	42	113	74	33	107	262	1.4	5.8	11	10.9	309	0.14	-42	-37	37
$Fe_2Ni_8$	1.76	7.35	8	101	109	51	73	182	1.5	8.6	4.6	6.2	413	0.19	-37	-41	39
$Ni_5$	0	4.53	51	89	129	22	165	326	1.0	2.4	19.2	18.1	n.a.	n.a.	n.a.	n.a.	n.a.
$Fe_5Ni_5^*$	Spent catalyst from isoeugenol hydrodeoxygenation without n-hexadecane (marked as IE + cat)																
$Fe_2Ni_8$	Spent catalyst from n-hexadecane hydroisomerization-hydrocracking without isoeugenol (marked as HXD + cat)																
													15	0.01	-97	-97	11
													209	0.14	-68	-58	26

\* ca.10% of metals have been leached when n-hexadecane was not present in the reaction mixture.

A higher uptake of hydrogen in  $\text{Fe}_2\text{Ni}_8$  compared to monometallic counterparts is probably related to different iron and nickel oxide speciation in these catalysts.

The metal contents determined by ICP-EOS, metal particle sizes (by TEM) and acidity from pyridine adsorption–desorption are summarized in Table 2, as they have a major impact on hydrodeoxygenation activity and selectivity and will be discussed in connection with the catalytic results. Worth noting is that introducing 5 wt% Fe on H-5.1 zeolitic support bearing mainly Brønsted acidity led to a decrease of strong acid sites and at the same time increased mainly medium Brønsted acid site, while introducing 5 wt% Ni led to significantly elevated weak and medium Lewis acid sites as will be discussed in a separate paper reporting in depth catalysts characterization.

In addition, Table 2 also displays characterization of the spent catalysts by TEM,  $\text{N}_2$  physisorption and TGA. Metal particle sizes distribution of Fe, Ni and Fe-Ni/H-Y-5.1 fresh and spent catalysts is shown in Fig. S2 while SEM images of the spent ones are displayed Fig. S3.

SEM images confirmed presence of well-defined zeolite crystallites, which retain their morphological structures after the metal introduction as well as after the reaction (4 h). For all catalysts, a comparison of the median particle size of both fresh and spent catalysts confirmed no sintering of metal particles during 4 h of co-processing at 573 K and 3 MPa of hydrogen. However, significant changes were observed in terms of the textural properties (Table 2). The maximum decrease in the specific surface area (more than 97%) and the pore volume (more than 85%) was recorded for the monometallic Fe catalyst, and for  $\text{Fe}_5\text{Ni}_5$ , which was used in isoeugenol hydrodeoxygenation without n-hexadecane (marked as IE + cat, Table 3). Other spent catalysts used in co-processing had the specific surface area and pore volume lower by 37–41% than the fresh ones. A larger decrease in textural properties (by 58–68%) was observed for  $\text{Fe}_2\text{Ni}_8$  used in n-hexadecane

hydroisomerization-hydrocracking experiment without the presence of isoeugenol (marked as HXD + cat, Table 3).

This decrease of the specific surface area of the catalyst was correlated with the coke formation, determined by TGA ( $m_{\text{coke}}$ ). Catalysts showing a lower decrease of the surface area revealed a higher amount of coke (Fig. 4a). At the same time, coke formation was increased with increasing Ni concentration and decreasing Fe concentration in the catalyst (Fig. 4b). A direct correlation with the FeNi particle sizes could not be established. However, it should be also mentioned, that in TEM images, nanoparticles of Fe and Ni could not be separated from each other in bimetallic catalysts. The observed effect of the metal nature on the coke formation is in line with [64] dealing with coke formation during the steam cracking of propane on foils of nickel and on a series of Ni-Cr-Ir alloys, showing that a substantially higher rate of coke formation was observed for the pure nickel foils. It should be also mentioned that deposited coke in the spent catalyst also linearly increased with decreasing amount of  $\text{Fe}^{3+}$  species determined in the bulk by Mössbauer spectroscopy in the fresh catalyst (Fig. S4a).

For Fe-based and Ni-based alloys [65,66] it was reported that carbon deposited over time is related to small metal particles (ca. 10 nm) generated through nickel disintegration, which occurs via a direct inward or internal growth of graphite (graphitisation).

According to the heat release during TGA, the coke was mostly oxidized in the 440–550 °C temperature region (Fig. S4b). In [67] a similar temperature range, 400–530 °C, was obtained pointing on the predominance of amorphous filamentous type coke formation for 2.5–10 wt% Ni-UGSO catalyst (Nickel-UpGraded Slug Oxides) in glycerol steam reforming.

In the current work, the extracted soluble coke species were identified by NMR (Fig. S5) and GC-MS (Fig. S5). Both methods confirmed predominated aliphatic coke (primary compounds: C10-C16 straight-chain alkanes) and a low amount of aromatics (primary component: dimethylethyl benzene). In the cases of the

**Table 3**

List of preliminary experiments: thermal experiments without a catalyst (entry 1–3), catalytic experiments with single substrates (entry 4–5), co-processing (6). Notation: IE – isoeugenol, racemic mixture; HXD – n-hexadecane; cat – catalyst.

Entry	Code	Catalyst	Isoeugenol	n-Hexadecane	IE/cat	HXD/cat	Conditions
1	IE	-	54 g	-	-	-	473 K, 2 MPa
2	HXD	-	-	77.3 g	-	-	573 K, 3 MPa
3	HXD + IE	-	0.2 g	77.3 g	-	-	573 K, 3 MPa
4	IE + cat	$\text{Fe}_5\text{Ni}_5$	1.0 g	56 g	56	-	473–573 K, 2 MPa
5	HXD + cat	$\text{Fe}_2\text{Ni}_8$	0.1 g	-	-	773	573 K, 3 MPa
6	HXD + IE + cat	$\text{Fe}_2\text{Ni}_8$	0.1 g	0.2 g	2	773	573 K, 3 MPa

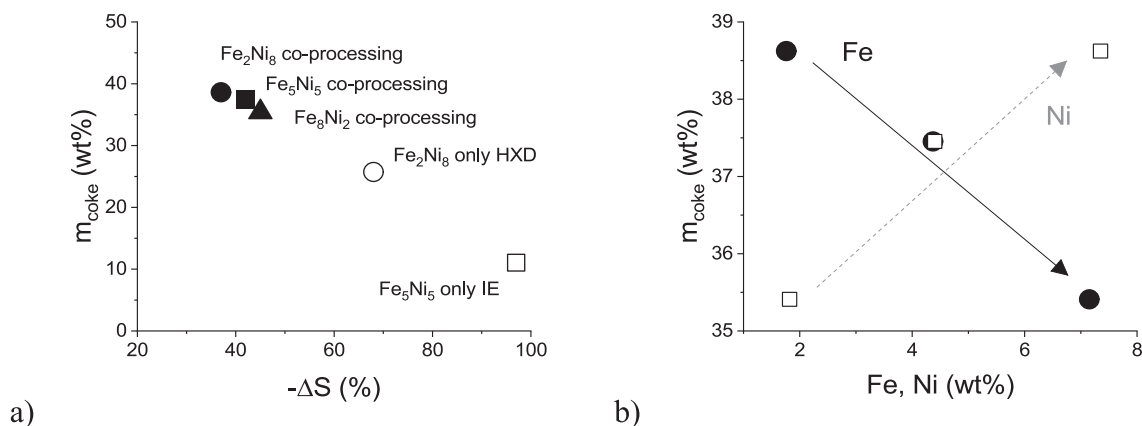


**Fig. 4.** Deposited coke in the spent catalyst as a function of: (a) decrease of the catalyst surface area, (b) metals concentration in the catalyst.

**Table 4**

Catalytic results of preliminary experiments after 4 h. All data are presented in mol%. Notation: IE – isoeugenol, racemic mixture. DHE – dihydroeugenol, HXD – n-hexadecane, cat – catalyst, X – conversion, MB – the liquid phase mass balance, CB – carbon balance, > C16 – alkylated hexadecane, i-C16 – isomerized hexadecane, C13-C15 – long-chain hydrocarbons, C8-C12 – jet fuels fraction, < C8 – cracked light hydrocarbons, NL – nonlinear products (branched and cyclic), L – linear products.

Entry	Code	Conversion			Balance		Yield	Selectivity					NL/L	
		X <sub>IE</sub>	X <sub>DHE</sub>	X <sub>HXD</sub>	MB	CB		Y <sub>total</sub>	> C16	i-C16	C13-C15	C8-C12	< C8	NL
1	IE	17	0	–	100	100	17	0	0	0	100	0	100	0
2	HXD	–	–	0.42	100	100	0.1	0	54	34	12	0	60	40
3	HXD + IE	97	0	0.03	100	100	0.3	0	9	2	86	2	89	11
4	IE + cat	100	3	–	99	98	98	0	0	0	100	0	100	0
5	HXD + cat	–	–	29	93	93	29	0.2	45	9	29	17	83	17
6	HXD + IE + cat	100	100	16	96	97	16	0.5	48	7	28	17	85	15

monometallic Ni and bimetallic Fe<sub>2</sub>Ni<sub>8</sub> catalysts, mainly n-hexadecane with a small amount of n-dodecane, dimethylethylbenzene, n-tridecane, n-tetradecane and methylpentadecane were detected (Fig. S5a). On the contrary in the cases of the bimetallic Fe<sub>5</sub>Ni<sub>5</sub> and Fe<sub>8</sub>Ni<sub>2</sub> catalysts, a slightly dominant component was aromatic dimethylethylbenzene with a broad distribution of aliphatic cokes (Fig. S5b).

Analysis of the spent catalyst by the solid state <sup>27</sup>Al NMR illustrated also changes with aluminium (Fig. S7). A peak at about –75 ppm has appeared being almost as large as the tetrahedral alumina peak at 59 ppm. The exact reason for this peak is not clear, but most probably it is associated with deposited coke and formation of Al-CR<sub>3</sub> species as proposed in [68].

### 3.2. Activity and selectivity of Fe, Ni and Fe-Ni/H-Y-5.1 catalysts

Co-processing of hexadecane with lignin derived isoeugenol as a model compound was investigated in this work using mono- and bimetallic iron and nickel supported on H-Y-5.1 zeolite. In order to understand the co-processing behaviour and the role of each compound in the mixture, in addition to the catalyst screening experiments, a set of additional experiments were performed. They comprised thermal experiments without a catalyst and catalytic experiments with single compounds (Table 3). Thermal and catalytic results of such experiments were summarized in Table 4.

#### 3.2.1. Preliminary experiments: Thermal experiments without a catalyst

After 4 h of the thermal experiment of isoeugenol (IE), only 17% of isoeugenol was hydrogenated to dihydroeugenol and no other products were detected (Table 4, entry 1). After 4 h of the thermal experiment with n-hexadecane (HXD), 0.42% of n-hexadecane was converted (Table 4, entry 2). The main products were isomers of hexadecane (i-C16 = 54%) followed by long-chain hydrocarbons (C13-C15 = 34%) while the jet fuels fraction of cracked product, C8-C12, was 12%. No cracked light hydrocarbons (<C8) or alkylated hexadecane (>C16) were detected. The ratio between branched and linear hydrocarbons was 1.5.

The thermal experiment with isoeugenol in n-hexadecane (HXD + IE) revealed almost zero conversion of n-hexadecane (X<sub>HXD</sub> = 0.03%) in the presence of even a small amount of isoeugenol (0.26 wt%, Table 3, Table 4, entry 3). On the contrary, hydrogenation of isoeugenol was accelerated in the diluted system at the expense of inhibited n-hexadecane transformations. However, it should be noted that a higher conversion of isoeugenol can be also related to a higher reaction temperature. The main products were the C8-C12 fraction (86%) consisting of 92% of dihydroeugenol and 8% of linear hydrocarbons. Selectivity to the isomerized hexadecane was only 9%.

The liquid phase mass balance and carbon balances of all thermal experiments without a catalyst was 100%.

#### 3.2.2. Preliminary experiments: Catalytic experiments with single substrates

The results of preliminary catalytic experiments over catalyst are displayed in Table 4. After 4 h at 573 K of the solventless isoeugenol hydrodeoxygenation over Fe<sub>5</sub>Ni<sub>5</sub> catalyst (IE + cat), the total conversion of isoeugenol was achieved, wherein only 3% of the formed dihydroeugenol was further converted to propylphenol (Table 4, entry 4). Low activity of the deoxygenation step can be related to the high reactant-to-catalyst ratio (56, Table 3, entry 4) and also catalyst deactivation due to coke formation. The latter one is in line with the analysis of the catalyst textural properties. While the specific surface area of the fresh catalyst was 530 m<sup>2</sup>/g, it was only 15 m<sup>2</sup>/g for the spent one (Table 2). From the recording of the process data (Fig. 5), it can be concluded that the catalyst deactivation probably occurs already in the first seconds of the experiment, when the preheated reactant comes into contact with the hot dry catalyst. After injecting the reactant into the reactor with a fresh hydrogen feed, a temperature drop to 315 K was observed, followed by an increase to 333 K.

Hydroisomerization-hydrocracking of n-hexadecane over Fe<sub>2</sub>Ni<sub>8</sub> catalyst (HXD + cat) revealed a relatively a high conversion, and the total yield of all products, 29%, with the content of branched and linear hydrocarbons 83 % vs 17 %, respectively (Table 4, entry 5). The main products were isomerized hexadecane (i-C16 = 48%, yield = 13.2%) followed by the jet fuels fraction of the cracked product (C8-C12 = 29%, yield = 8.6%). At the same conversion level of n-hexadecane, 30%, the same selectivity to i-C16, 49%, was obtained over 0.1 g Pt/ZSM-48 catalyst [54] and significantly lower, 20 % of i-C16 selectivity over Pt/ZSM-23 dual template [69] at the same temperature 573 K and a higher hydrogen pressure 4 MPa in a fixed-bed reactor. Over the monometallic 7.6 wt % Ni/H-MFI (18.5 nm) and 9.1 wt% Ni/Beta (11.4 nm) catalyst, selectivity to i-C16 was 0 and 56.6% at a significantly higher conversion of 95% and 64%, respectively, in the fixed-bed reactor at the same pressure 30 bar and lower temperature 548 K [70]. For Ni/ZSM-48 catalysts exposed to different alkali treatment, selectivity to i-C16 was ca. 25–35% at ca. 70–85% of conversion in the fixed-bed reactor at the same temperature [71]. Compared to the thermal experiment, the cracked light hydrocarbons (<C8 of 17%) and small amounts of alkylated hexadecane (>C16 of 0.2%) were also detected in the current work. On the contrary, selectivity to the long-chain hydrocarbons decreased from 34% to 9%. Comparison with more expensive noble metal-supported catalysts [50] showed comparable results in terms of the yield of jet fuels fraction at the same conversion level of n-hexadecane, 30%. However, it should be noted that such comparison is not straightforward as the experiments were conducted under different conditions and the jet fuels fraction was defined by C9–C15 in [50]. The experi-

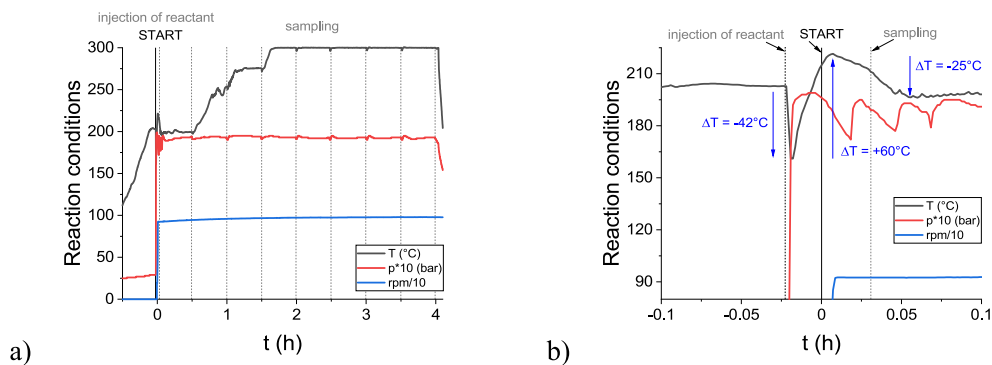


**Fig. 5.** Solventless isoeugenol hydrodeoxygenation (a) full scale and (b) zoom-in of reaction conditions in time. Conditions: 52 mL of the reaction volume, 1 g of  $\text{Fe}_5\text{Ni}_5$  catalyst, and the weight ratio of reactant-to-catalyst of 56 at 473–573 K and 2 MPa of hydrogen. The preheated reactant was injected on the hot dry catalyst. The start of the reaction corresponds to the initiation of mixing.

ments in [50] were carried out at a lower temperature, 513 K (573 K in the current work), higher pressure of hydrogen (4.5 vs 3 MPa in the current work) and a significantly lower ratio of reactant-to-catalyst, 23 (773 here). The yield of the jet fuels fraction defined as C9–C15 over compared catalysts decreased in the following order: 16% (2.5 wt% Ru/H-Beta-300,  $d_{\text{Ru}}$  of 17 nm, total acid sites (TAS) 241  $\mu\text{mol/g}$ , [50]) >9% ( $\text{Fe}_2\text{Ni}_8$ ,  $d_{\text{Fe-Ni}}$  of 4.6 nm, TAS 182  $\mu\text{mol/g}$ , the current work) >4% (2.5 wt% Pt/H-Beta-25,  $d_{\text{Pt}}$  3.3 nm, TAS 388  $\mu\text{mol/g}$ , [50]).

Co-processing of isoeugenol and n-hexadecane over  $\text{Fe}_2\text{Ni}_8$  catalyst (**HXD + IE + cat**) was performed with 0.1 g of  $\text{Fe}_2\text{Ni}_8$  catalyst (Table 3, entry 6). The amount of isoeugenol in n-hexadecane was the same as for the non catalytic experiment, i.e. 0.26 wt%. Full conversion of both isoeugenol and dihydroeugenol and 15.5% of n-hexadecane conversion was obtained after 4 h at 573 K and 3 MPa. In the case of hydrodeoxygenation, a significantly faster reaction can be mainly attributed to a lower ratio of the reactant-to-catalyst, 2, in the diluted system and negligible catalyst deactivation in the first seconds of the process. After 4 h, the specific surface area and the total pore volume of the catalyst decreased only by 37% and 41%, respectively (Table 2). In this case, both compounds (isoeugenol, n-hexadecane) and the catalyst were loaded into the reactor at room temperature and heated up to the reaction temperature with the heating rate of 10 K/min. This procedure was used for all catalyst screening experiments (Section 3.1.3). Just a half n-hexadecane conversion compared to the experiment without isoeugenol can be related to the strong adsorption of cyclic compounds on the surface of catalyst and to the faster isoeugenol hydrodeoxygenation in diluted system what points out on the competitive reactions in co-processing (Table 4, entry 5 and 6). This is also in line with results from the thermal experiment with 0.26 wt% of isoeugenol in n-hexadecane (**HXD + IE**). The ratio between nonlinear (branched and cyclic) and linear products was 85% vs 15%, respectively, in this catalytic co-processing. Selectivity based on the carbon number was close to the results for the experiment without isoeugenol, i.e. only slightly higher selectivity to alkylated and isomerized hexadecane and slightly lower selectivity to long-chain hydrocarbons was observed.

A lower liquid phase mass balance and carbon balances 93–99% could be related to the light cracked hydrocarbons in the gas phase, and adsorption of heavy compounds on the catalyst, coke formation. The latter one is in line with the textural properties of the spent catalyst (Table 2). Worth also noting that ca 1.8-fold higher deactivation of  $\text{Fe}_2\text{Ni}_8$  surface (Table 2) was observed in the experiment without isoeugenol, i.e. **HXD + cat**, compared to the one with this compound, **HXD + IE + cat**. This reflects 1.8-fold higher n-hexadecane conversion for isoeugenol free experiment, **HXD + cat**

(Table 4, entry 5 and 6). An analogous competition was found for tetralin and a phenolic compound in their co-processing over a commercial FCC catalyst [45].

### 3.2.3. Products distribution of the preliminary experiments

Distribution of all products according to the carbon number is presented in Fig. S8. Experiments with isoeugenol without n-hexadecane (**IE, IE + cat**) showed a maximum at C10, which is obviously related to isoeugenol and dihydroeugenol. The thermal experiment of n-hexadecane (**HXD**) exhibited a maximum at C13 of linear tridecane, followed by the second maximum of methyl-nonane, C10. In n-hexadecane hydroisomerization-hydrocracking over  $\text{Fe}_2\text{Ni}_8$  (**HXD + cat**) the same shape of the product distribution of C3–C14 showing preferential cracking in the middle of the hexadecane hydrocarbon chain, i.e. symmetrical and centred at C8, has observed in line with the previous work with platinum based catalysts Pt/ZrO<sub>2</sub> [72], Pt/Al-MCM-48 [73], and Pt/H-Y-30A [73]. In [73,74], selectivity toward cracking in the middle of the carbon chain was supported by small (2–8 nm) mesopores in the crystals. This selectivity shift was attributed to an enhanced mass transfer and faster desorption of the primary products due to a shorted diffusion path, limiting thus subsequent cracking. It should be noted, that,  $\text{Fe}_2\text{Ni}_8$  catalyst, in the current work, comprised mainly micropores (<2 nm, 73%). In the case of the monometallic Ni catalysts, the maximum selectivity for hydrocarbons below C15 was obtained for C5–C10 fraction, namely 60%, with 7.6 wt% Ni/H-MFI (<2 nm, 76%) and for C11–C15 fraction, 30%, with 9.1 wt% Ni/Beta (<2 nm, 23%) [70].

A similar profile was also observed in the co-processing (**HXD + IE + cat**) displaying a small additional maximum at C9 related to the products from isoeugenol hydrodeoxygenation. Overall, the highest maximum at C16 represents the highest selectivity to methyl-pentadecane of 45 and 48% in the experiment without (**HXD + cat**) and with isoeugenol (**HXD + IE + cat**), respectively.

Distribution of the linear hydrocarbons according to the carbon number (Fig. 6) clearly showed that the presence of the catalyst led to significant n-hexadecane cracking to the light hydrocarbons. Fig. 7 displaying the linear product distribution as a function of reaction time, revealed only minor changes after 30 min.

### 3.2.4. Catalyst screening: conversion, reaction rates and turnover frequency

The synergistic effect of Fe and Ni supported on H-Y-5.1 zeolite in the co-processing of n-hexadecane with isoeugenol was investigated over five catalysts with different Fe/Ni ratios in a batch reactor at 573 K and 3 MPa of hydrogen (Fig. 9, Table 5).

The n-hexadecane conversion and the reaction rate decreased with the increasing metals particle size. Especially, the particle size

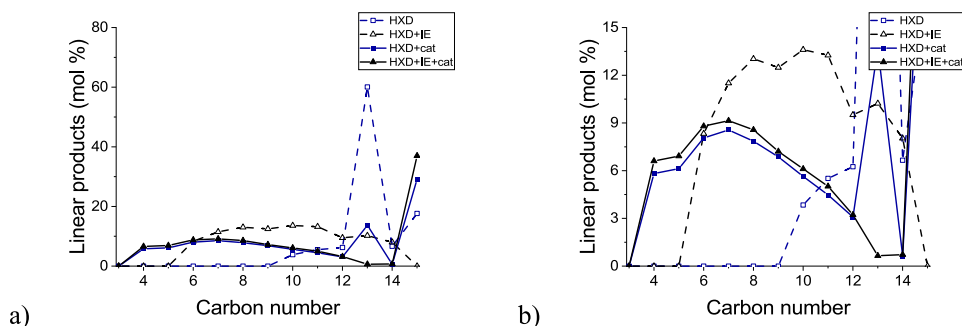


Fig. 6. Distribution of linear products (molar fraction) after 4 h as a function of the carbon number for experiments in Table 4: (a) full scale and (b) zoom-in.

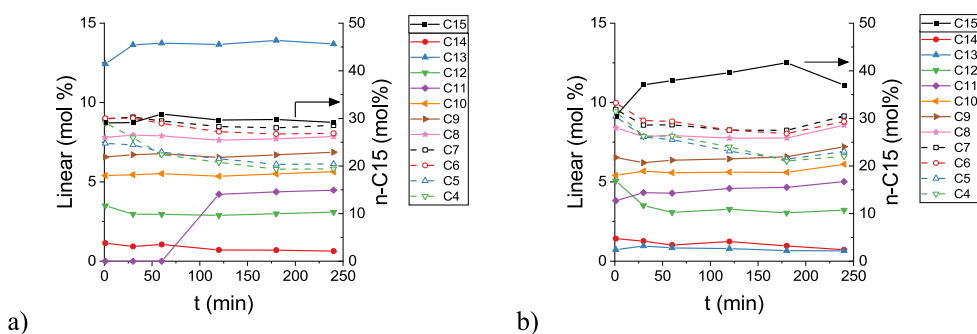


Fig. 7. Linear product distribution (molar fraction) as a function of reaction time in: (a) n-hexadecane hydroisomerization-hydrocracking over Fe<sub>2</sub>Ni<sub>8</sub> catalyst (HXD + cat) and (b) co-processing of isoeugenol hydrodeoxygenation and n-hexadecane hydroisomerization-hydrocracking over Fe<sub>2</sub>Ni<sub>8</sub> catalyst (HXD + IE + cat). Conditions: 573 K and 3 MPa of hydrogen with 100 mL of the reaction volume, 0.1 g of catalyst.

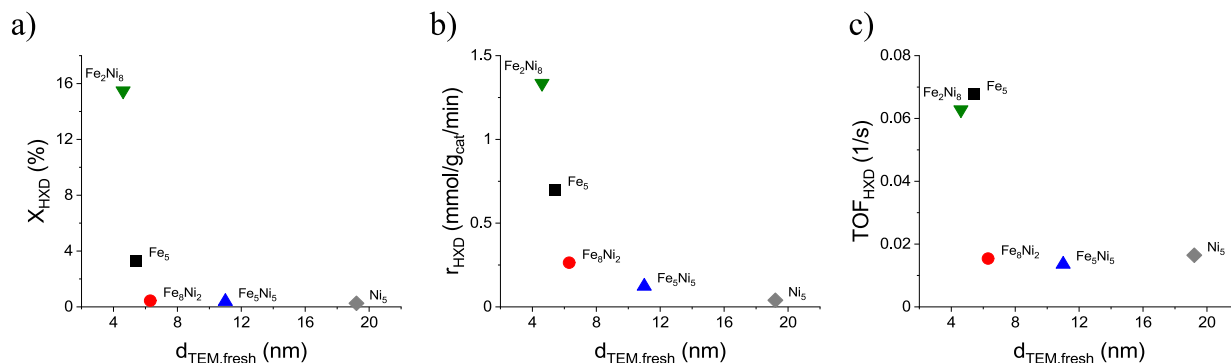


Fig. 8. Co-processing isoeugenol with n-hexadecane: (a) conversion after 4 h, (b) reaction rate, (c) initial turnover frequency of n-hexadecane as a function of the median Fe-Ni particle size (determined by TEM). Conditions: 573 K and 3 MPa of hydrogen with 100 mL of the reaction volume, 0.1 g of catalyst, and the weight ratio of reactant-to-catalyst of 2 and 773 with respect to isoeugenol and n-hexadecane, respectively. Legend: no catalyst, n-hexadecane with isoeugenol (+), Fe<sub>5</sub> (black ■), Fe<sub>3</sub>Ni<sub>2</sub> (red ●), Fe<sub>2</sub>Ni<sub>8</sub> (blue ▲), Fe<sub>2</sub>Ni<sub>8</sub> (green ▼), Ni<sub>5</sub> (grey ◆). (For interpretation of the references to colour in this figure legend, the reader is referred to the web version of this article.)

smaller than 6 nm exhibited a positive influence on the reaction (Fig. 8a,b). In addition, the results of n-hexadecane hydroisomerization-hydrocracking pointed out on the structure insensitivity for the catalysts at least with the median Fe-Ni particle size larger than 5.5 nm as beyond this size the turnover frequency (TOF) was constant (Fig. 8c).

These results are in line with the literature [50], where the reaction rate of n-hexadecane (0.001–0.045 mmol/g/min) hydrocracking also decreased with increasing metal particle sizes independent on the metal nature, namely Pt, Ni or Ru. A comparison of the monometallic Ni-catalysts showed that the reaction rate of 0.045 mmol/g/min over 5 wt% Ni/H-Beta-150 (9.4 nm) in an autoclave at a lower temperature of 483 K and a higher pressure of 4 MPa was comparable to the reaction rate of 0.04 mmol/g/min over Ni<sub>5</sub> (19.2 nm) in the current work in the presence of isoeu-

genol. Simultaneously, the reaction rate of n-hexadecane in the presence of isoeugenol with Fe<sub>5</sub>Ni<sub>5</sub> ( $2.1 \cdot 10^{-6}$  mol/g/s) was comparable with the reaction rate obtained in the fixed-bed reactor at a lower temperature of 513 K and a lower pressure of 2 MPa over Pt/H-Y30A ( $1.8 \cdot 10^{-6}$  mol/g/s) and Pt/Al-MCM-48 ( $1.7 \cdot 10^{-6}$  mol/g/s) catalysts with a sieved fraction of 180–425  $\mu\text{m}$  and Pt particle size of  $<3$  nm [73]. Compared to the monometallic Ni-catalyst in the current work, ca. two-fold lower TOF of n-hexadecane (29 1/h) was obtained in the fixed-bed microreactor at a higher temperature of 613 K and 2 MPa over NiW/Ni-SAPO-11 catalysts with a sieved fraction of 400–840  $\mu\text{m}$ , with the 5 and 15 wt% loading of NiO and WO<sub>3</sub>, respectively [75].

No clear correlation between the turnover frequency, normalized either per total amount of acid sites or sites of different strength on one hand and the acid site density on the other hand,

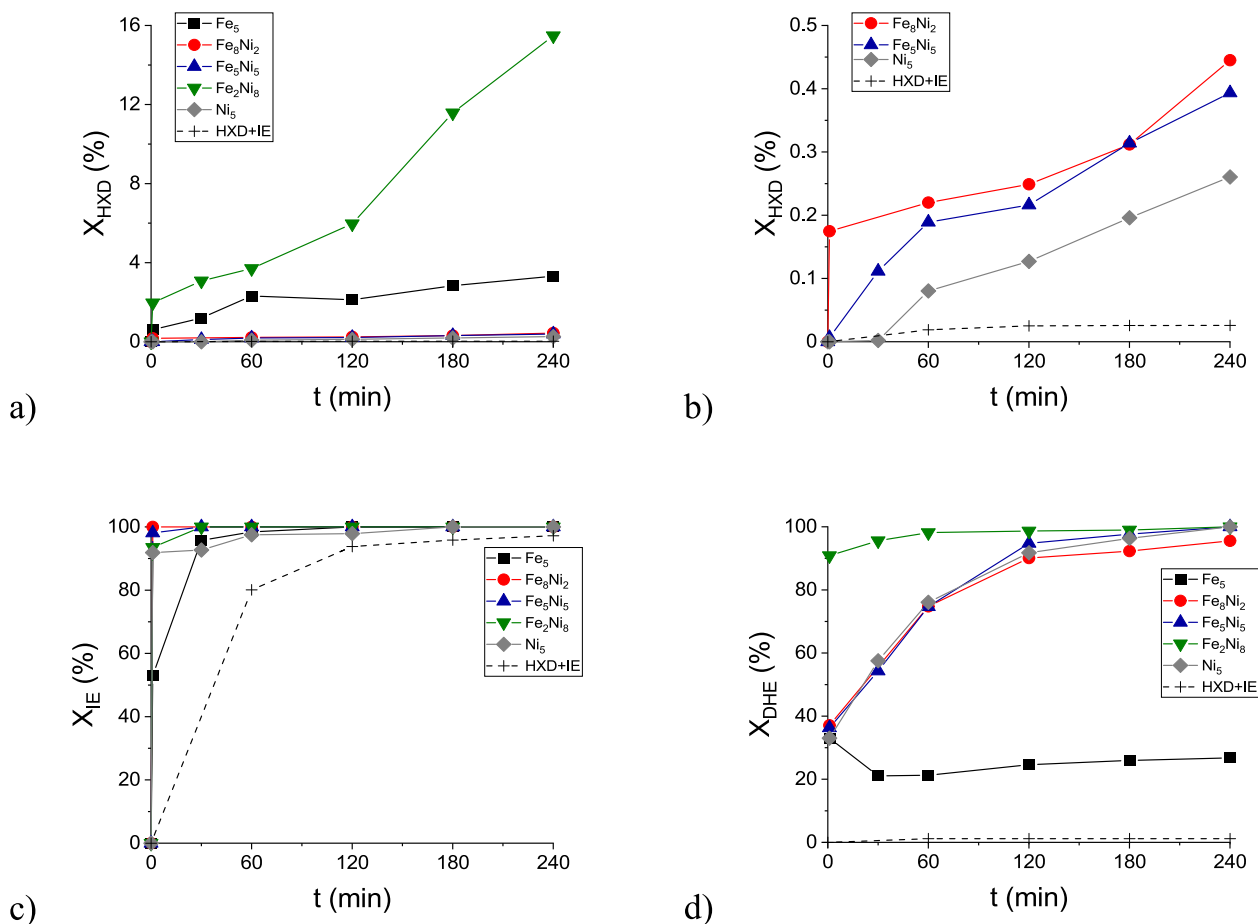


**Fig. 9.** Co-processing of isoeugenol with n-hexadecane: (a,b) full scale and zoom-in of n-hexadecane conversion, (c) isoeugenol conversion, (d) dihydroeugenol conversion, as a function of the reaction time. Conditions: 573 K and 3 MPa of hydrogen with 100 mL of the reaction volume, 0.1 g of catalyst, and the weight ratio of reactant-to-catalyst of 2 and 773 with respect to isoeugenol and n-hexadecane, respectively. Legend: no catalyst, n-hexadecane with isoeugenol (+), Fe<sub>5</sub> (black ■), Fe<sub>8</sub>Ni<sub>2</sub> (red ●), Fe<sub>5</sub>Ni<sub>5</sub> (blue ▲), Fe<sub>2</sub>Ni<sub>8</sub> (green ▼), Ni<sub>5</sub> (grey ◆). (For interpretation of the references to colour in this figure legend, the reader is referred to the web version of this article.)

**Table 5**

Catalytic results of catalyst screening after 4 h. All data are presented in mol%. Notation: IE – isoeugenol, racemic mixture, DHE – dihydroeugenol, HXD – n-hexadecane, cat – catalyst, X – conversion, MB – the liquid phase mass balance, CB – carbon balance, > C16 – alkylated hexadecane, i-C16 – isomerized hexadecane, C13–C15 – long-chain hydrocarbons, C8–C12 – jet fuels fraction, C8–C12\* – jet fuels fraction without dihydroeugenol, < C8 – cracked light hydrocarbons, NL – nonlinear products (branched and cyclic), L – linear products, PC – phenolic compounds, OFBD – oxygen-free benzene derivatives, OFCAD – oxygen-free cycloalkane derivatives. Conditions: 573 K and 3 MPa of hydrogen with 100 mL of the reaction volume, 0.1 g of catalyst, and the weight ratio of reactant-to-catalyst of 2 and 773 with respect to isoeugenol and n-hexadecane, respectively.

Catalyst	Conversion			Balance		Yield		Selectivity					NL/L		Cyclic products distribution			
	X <sub>IE</sub>	X <sub>DHE</sub>	X <sub>HXD</sub>	MB	CB	Y <sub>total</sub>	Y <sub>C8–C12*</sub>	> C16	i-C16	C13–C15	C8–C12	< C8	NL	L	DHE	PC	OFBD	OFCAD
Fe <sub>5</sub>	100	27	3.32	97	97	0.16	0.01	0	14	6	76	4	84	16	100	0	0	0
Fe <sub>8</sub> Ni <sub>2</sub>	100	96	0.45	100	100	0.63	0.12	15	46	8	21	10	86	14	5	13	38**	44
Fe <sub>5</sub> Ni <sub>5</sub>	100	100	0.39	100	100	0.43	0.15	0	44	12	36	9	82	18	0	0	19	81
Fe <sub>2</sub> Ni <sub>8</sub>	100	100	15.48	96	97	15.80	4.50	0.5	48	7	28	17	85	15	0	10	8	82
Ni <sub>5</sub>	100	100	0.26	100	100	0.57	0.14	0	47	14	25	14	80	20	0	5	7	88

Y<sub>C8–C12\*</sub> – yield of jet fuels fraction without dihydroeugenol, \*\* – oxygen-free benzene and tetralin derivatives.

could be visible as follows from Fig. S9. Some reactions catalysed by solid acids, such as for example pentane cracking and dehydration of various alcohols over metal-free H-MFI catalysts with different Brønsted acid sites [76], displayed clear correlations between TOF and Brønsted acid site density. Apparently absence of correlations between TOF and the acid site density in the current work could be attributed to complexity of n-hexadecane hydroisomerization-hydrocracking reaction occurring over bifunctional/bimetallic catalysts and involving besides acid sites also the metal sites.

Overall, it can be concluded, that lower activity of n-hexadecane hydroisomerization-hydrocracking in co-processing was comparable with the results of the single processes obtained at milder reaction conditions, with a larger metal particle size or in the presence of mass transfer limitations.

The conversion data for catalytic and for comparison also non-catalytic experiments, of both processes, are displayed in Fig. 9. Except for the monometallic Fe catalyst, hydrogenation of isoeugenol was very rapid, and almost complete transformation to dihydroeugenol was already observed in the first minute of

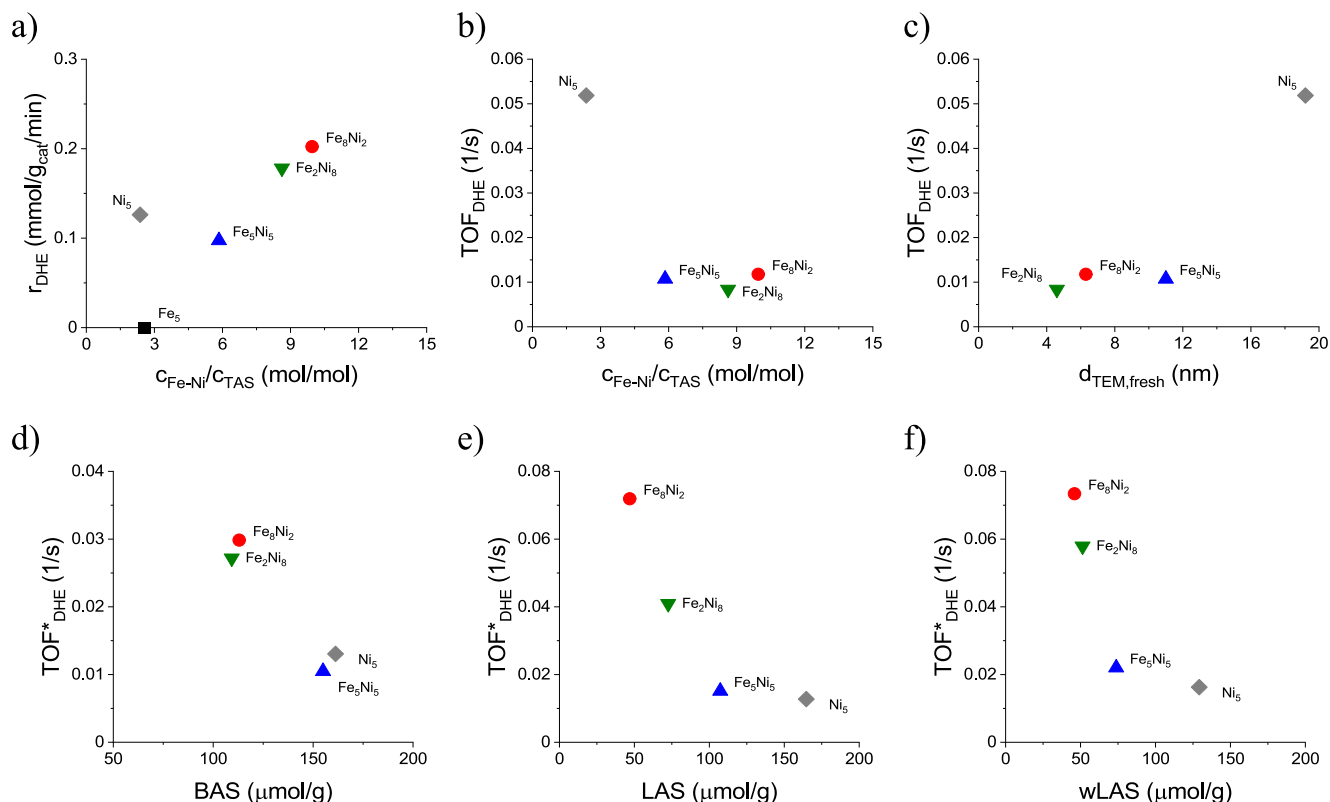


**Fig. 10.** Co-processing of isoeugenol with *n*-hexadecane: (a) reaction rate, (b) initial turnover frequency of dihydroeugenol as a function of the molar ratio of metals-to-acid site, (c) initial turnover frequency of dihydroeugenol as a function of the median Fe-Ni particle size (determined by TEM), (d) initial turnover frequency of dihydroeugenol as a function of the total Brønsted acid sites, (e) initial turnover frequency of dihydroeugenol as a function of the total Lewis acid sites, (f) of the weak Lewis acid sites. Conditions: 573 K and 3 MPa of hydrogen with 100 mL of the reaction volume, 0.1 g of catalyst, and the weight ratio of reactant-to-catalyst of 2 and 773 with respect to isoeugenol and *n*-hexadecane, respectively. Legend: no catalyst, *n*-hexadecane with isoeugenol (+), Fe<sub>5</sub> (black ■), Fe<sub>8</sub>Ni<sub>2</sub> (red ●), Fe<sub>5</sub>Ni<sub>5</sub> (blue ▲), Fe<sub>2</sub>Ni<sub>8</sub> (green ▼), Ni<sub>5</sub> (grey ◆). (For interpretation of the references to colour in this figure legend, the reader is referred to the web version of this article.)

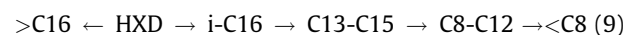
the co-processing with all catalysts. This result was analogous to the results reported for the supported Ni catalysts in [26]. It should be also pointed out that the reaction proceeds via rapid hydrogenation to dihydroeugenol (Fig. 9a, Table 4), even in the absence of any catalyst, which is in line with the literature [40]. Therefore, Fig. 9 also displays conversion of the consecutive step, i.e. conversion of dihydroeugenol.

In the case of hydrodeoxygenation, the results clearly showed that the bifunctional nature of the metal–acid catalysts has a key role. The reaction rate of dihydroeugenol linearly increased with the increasing molar ratio of the metals-to-total acid site ( $C_{\text{Fe-Ni}}/C_{\text{TAS}}$ ). The exception was the monometallic Ni-catalyst (Fig. 10a), which could be explained by the absence of oxophilic

iron in this catalyst compared to other ones. A significant role of catalyst bifunctionality is in line with [77], where the best catalytic behaviour in guaiacol hydrodeoxygenation exhibited by 15.7 wt% Ni/Beta-12.5 (9.2 nm), was attributed to the optimized balance between active hydrogenation (metal) and acid sites with  $C_{\text{Ni}}/C_{\text{TAS}}$  of 3.8. In the current work, for the bimetallic Fe-Ni catalyst, the turnover frequency, defined by exposed moles of metals, was independent on  $C_{\text{Ni-Fe}}/C_{\text{TAS}}$  and also on the metal particle size (Fig. 10b, c), while the turnover frequency, defined by Brønsted and Lewis acid sites (total, respectively weak), decreased with increasing Brønsted and Lewis acidity (Fig. 10d,e,f).

### 3.2.5. Catalyst screening: Product distribution

Furthermore, the results from the catalyst screening experiments also clearly showed that not only the reaction rates, but also the product distribution strongly depends on the Fe-Ni metals ratio in the catalysts (Table 5). The reported results of product distribution reflect the simplified reaction schemes of both processes, *n*-hexadecane hydroisomerization-hydrocracking (Eq. (9)) and isoeugenol hydrodeoxygenation (Fig. 11):



where  $>C16$  is alkylated hexadecane, HXD is *n*-hexadecane, i-C16 is isomerized hexadecane, C13–C15 are long-chain hydrocarbons with 13–15 carbon atoms, C8–C12 is jet fuels fraction,  $<C8$  are cracked light hydrocarbons.

Extremely slow isoeugenol hydrodeoxygenation over the monometallic Fe catalyst resulted in only 27% of dihydroeugenol conversion and relatively rapid *n*-hexadecane

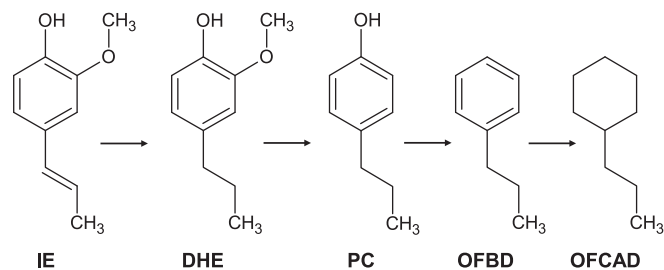


**Fig. 11.** A simplified reaction scheme of isoeugenol hydrodeoxygenation. Legend: IE - isoeugenol, DHE - dihydroeugenol, PC - phenolic compounds (e.g. 4-propylphenol in the scheme), OFBD - oxygen-free benzene derivatives (e.g. propylbenzene in the scheme), OFCAD - oxygen-free cycloalkane derivatives (e.g. propylcyclohexane in the scheme).

hydroisomerization-hydrocracking with the second highest conversion of 3.3%. It should be noted that no other cyclic products were detected in the reaction mixture. This incomplete balance of cyclic products could be explained by a very low concentration of cyclic products (below the detection limit of GC-FID, MS) or strong adsorption of dihydroeugenol on the surface of the catalyst. The latter one is in line with the textural properties of the spent catalyst showing an extremely low specific surface area of 9 m<sup>2</sup>/g and the pore volume of 0.03 cm<sup>3</sup>/g (Table 2), i.e. by 98%, respectively, 85%, lower compared to the fresh catalyst. The rapid n-hexadecane hydroisomerization-hydrocracking could be attributed to the extra framework Al species (determined by solid state <sup>27</sup>Al MAS NMR just for the monometallic Fe catalyst as a small peak at 0 ppm). This is in line with [78], where it was observed that isomerization, cracking and related coking processes were favoured with increasing extra framework Al, while octanoic acid conversion decreased in hydrodeoxygenation over 5 wt% Ni/Al-SBA-15 catalysts.

Overall, it can be concluded that activity of the monometallic Fe catalyst in isoeugenol hydrodeoxygenation step was low and the results were comparable with an experiment without the catalyst (IE, Table 4). This result is interpreted by an insufficient hydrogenation ability of iron [79].

On the contrary, very high activity of dihydroeugenol transformation and at the same time of n-hexadecane was observed over Fe<sub>2</sub>Ni<sub>8</sub> catalyst in the first minutes compared to other catalysts (Fig. 9). Almost complete transformation of dihydroeugenol (>98%) was obtained after 60 min, which could lead to acceleration of n-hexadecane hydroisomerization-hydrocracking (from 2.3% to 5.6% conversion per hour). After 4 h, the total conversion of isoeugenol, and dihydroeugenol, as well as 15.5% of n-hexadecane conversion was achieved with the highest total yield of 15.8% and the highest yield of jet fuels fraction without dihydroeugenol of 4.5%. However, it should be noted, that cyclic products still contained some of the undesired oxygen-containing phenolic compounds. Characterization data, namely EXAFS and TPR profiles of fresh catalysts, pointed out on Fe-Ni interactions in bimetallic catalysts, which can be involved in explanation of catalytic behaviour. Strong interactions, compared to other materials, were obtained especially for the most active Fe<sub>2</sub>Ni<sub>8</sub> catalyst, according to the largest deviations of H<sub>2</sub>-TPR profile (Fig. 1).

According to FT EXAFS Fe<sub>2</sub>Ni<sub>8</sub> spectra (Fig. S12) the interatomic distances and the mean-square deviations of interatomic distances around Fe and Ni atoms are identical being slightly lower compared to the bulk fcc Ni metal. This, and the fact that a bcc lattice is typical for pure Fe nanoparticles, can imply a nearly random fcc alloy comprising Fe and Ni.

Moreover, Fe<sub>2</sub>Ni<sub>8</sub> catalyst comprising more Ni than Fe exhibited the smallest Fe-Ni particle sizes (4.6 nm, Table 2), the lowest amount of Brønsted acid sites (109 μmol/g, Table 2), the highest specific surface area (660 m<sup>2</sup>/g) and the highest amount of Fe metallic species in the bulk (43%). The results for Fe<sub>2</sub>Ni<sub>8</sub> are in line with the mechanism for which hydrodeoxygenation of phenolic components starts with partial hydrogenation of the aromatic ring giving propylcyclohexenol followed by this enol transformations to propylcyclohexanone and its subsequent hydrogenation to propylcyclohexanol, which can be easily dehydrated [26]. Furthermore, the bond energy for breaking OH group from the phenyl ring is 472 kJ/mol [80], being higher than that of aliphatic C–O, which is 393 kJ/mol [81].

The other three catalysts (Fe<sub>8</sub>Ni<sub>2</sub>, Fe<sub>5</sub>Ni<sub>5</sub> and Ni<sub>5</sub>) showed almost the same catalytic activity. Only slightly lower dihydroeugenol conversion was obtained over Fe<sub>8</sub>Ni<sub>2</sub> and a slightly lower n-hexadecane conversion over the monometallic Ni catalyst. On the contrary, the product distribution was significantly different for these catalysts compared to other materials. Selectivity to

alkylated hexadecane, >C16, was 15% for Fe<sub>8</sub>Ni<sub>2</sub>, while for others it was close to zero. The main product of hexadecane alkylation was eicosane, C20. At the same time, this catalyst exhibited the highest ratio between nonlinear (branched and cyclic) and linear products (NL/L) equal to 6.2. In addition, exclusively for this catalyst, tetralin derivatives were produced, and in a significant amount (35% from all cyclic compounds, Table 5). This can be related to the ring-closure over the weak Lewis acid sites as was described previously for cyclization of 5-phenyl-1-entene to 1-methyl-tetraline over FeCl<sub>3</sub> catalyst [82]. Although the Fe<sub>8</sub>Ni<sub>2</sub> catalyst contained the lowest absolute amount of weak Lewis acid sites compared to others, this catalyst exhibited the highest fraction of weak Lewis sites (98%), i.e. with a negligible amount of medium and no strong Lewis acid sites (Table 2). At the same time, this catalyst had the highest concentration of Fe among the bimetallic ones. A similar mechanism of ring closing was suggested for the Friedel-Crafts reaction between benzene and succinic anhydride using aluminium chloride [83] or the intermolecular Friedel-Crafts reaction of benzyl carbinols mediated over stoichiometric amounts of Lewis and Brønsted acids [84]. Tetralin derivatives were also formed in depolymerisation of polyethers with aromatic compounds using titanium-exchanged montmorillonite catalyst [85].

The lowest NL/L ratio of 4.1 was obtained with the monometallic Ni catalyst. Selectivity to isomerized hexadecane in co-processing (S<sub>iC16</sub> = 47% at X = 0.3%, Table 5), was comparable with the monometallic 10 wt% Ni/H-Beta (S<sub>iC16</sub> = 57% at X = 64%) and 10 wt% Ni/desilicated H-Beta (S<sub>iC16</sub> = 44% at X = 83.3%) catalysts with the smaller particle sizes of Ni, 11.4 and 16.7 nm, respectively, investigated in n-hexadecane hydroisomerization-hydrocracking in the trickle-bed reactor under the same pressure and slightly lower temperature of 548 K [70]. High conversion of hexadecane of 91% but a lower selectivity to i-C16 was obtained over 5 wt% Ni/WO<sub>3</sub>/ZrO<sub>2</sub> in the trickle-bed reactor under the same temperature of 573 K and a lower pressure of 2 MPa [86]. This Ni<sub>5</sub> catalyst also exhibited the highest selectivity to the long-chain hydrocarbons, C13–C15 and 5% of oxygen-containing cyclic products from all cyclic products.

In contrast, no oxygen-containing cyclic products were detected for Fe<sub>5</sub>Ni<sub>5</sub> catalyst. The cyclic compounds were composed of 19% oxygen-free benzene derivatives and 81% oxygen-free cycloalkane derivatives. The same catalyst displayed the highest selectivity to jet-fuel fraction, C8–C12. Fe<sub>5</sub>Ni<sub>5</sub> catalyst containing equal amounts of Fe as Ni exhibited Fe and Ni particle sizes of < 3 and 9 nm, respectively, a low Brønsted to Lewis acid sites ratio of 1 (Table 2), the lowest blocking temperature respectively the highest magnetic saturation (8.5 Am<sup>2</sup>/kg), and the highest hydrogen consumption in temperature programmed desorption (4.2 relative peak area) compared to other studied materials.

Overall, it can be concluded that dihydroeugenol conversion and selectivity to nonlinear cracked light hydrocarbons, <C8, increased with increasing Ni fraction in the catalysts. On the contrary, selectivity to a linear C14 hydrocarbon, n-tetradecane, decreased when there was more Ni in the catalyst. Except the monometallic Fe catalyst, the isomerized hexadecane, i-C16, was main product with selectivity of 44–48%. The fractions of nonlinear (branched and cyclic) and linear products were relatively close for all catalysts, namely 80–86% and 14–20%, respectively.

Selectivity to isomerized hexadecane, i-C16, and to the jet-fuel fraction, C8–C12, as a function of conversion is displayed in Fig. 12. From the results obtained at low conversion, where selectivity was changed with conversion, a network of consecutive reactions is much more prominent. In contrast, from almost constant selectivity obtained for Fe<sub>5</sub> and Fe<sub>2</sub>Ni<sub>8</sub> catalysts at high conversion, a reaction network with parallel reactions can be expected. The highest initial selectivity to jet fuel products, S<sub>C8–C12</sub>, among bimetallic

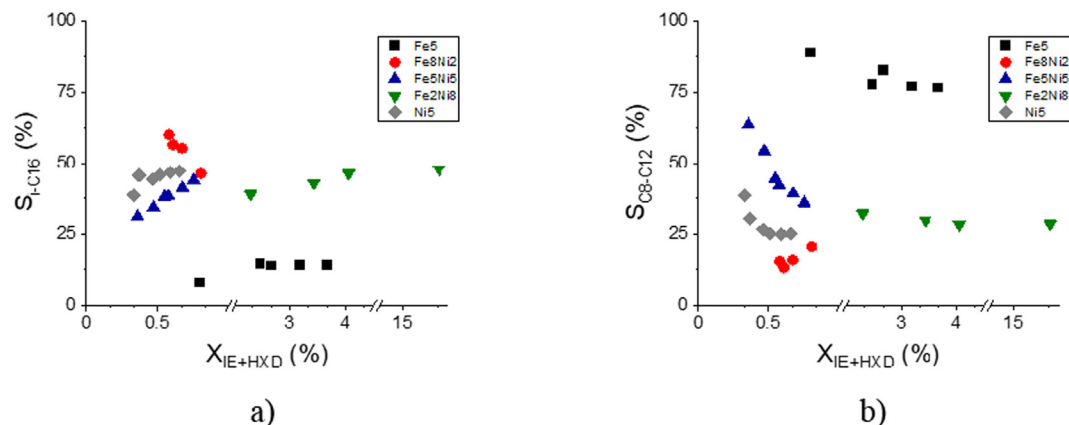


**Fig. 12.** Co-processing of isoeugenol with n-hexadecane: (a) selectivity to n-hexadecane isomers, (b) selectivity of jet-fuel hydrocarbons (C8–C12) as a function of co-processing conversion (Eq. (4)). Conditions: 573 K and 3 MPa of hydrogen with 100 mL of the reaction volume, 0.1 g of catalyst, and the weight ratio of reactant-to-catalyst of 2 and 773 with respect to isoeugenol and n-hexadecane, respectively. Legend: no catalyst, n-hexadecane with isoeugenol (+), Fe<sub>5</sub> (black ■), Fe<sub>8</sub>Ni<sub>2</sub> (red ●), Fe<sub>5</sub>Ni<sub>5</sub> (blue ▲), Fe<sub>2</sub>Ni<sub>8</sub> (green ▼), Ni<sub>5</sub> (grey ◆). (For interpretation of the references to colour in this figure legend, the reader is referred to the web version of this article.)

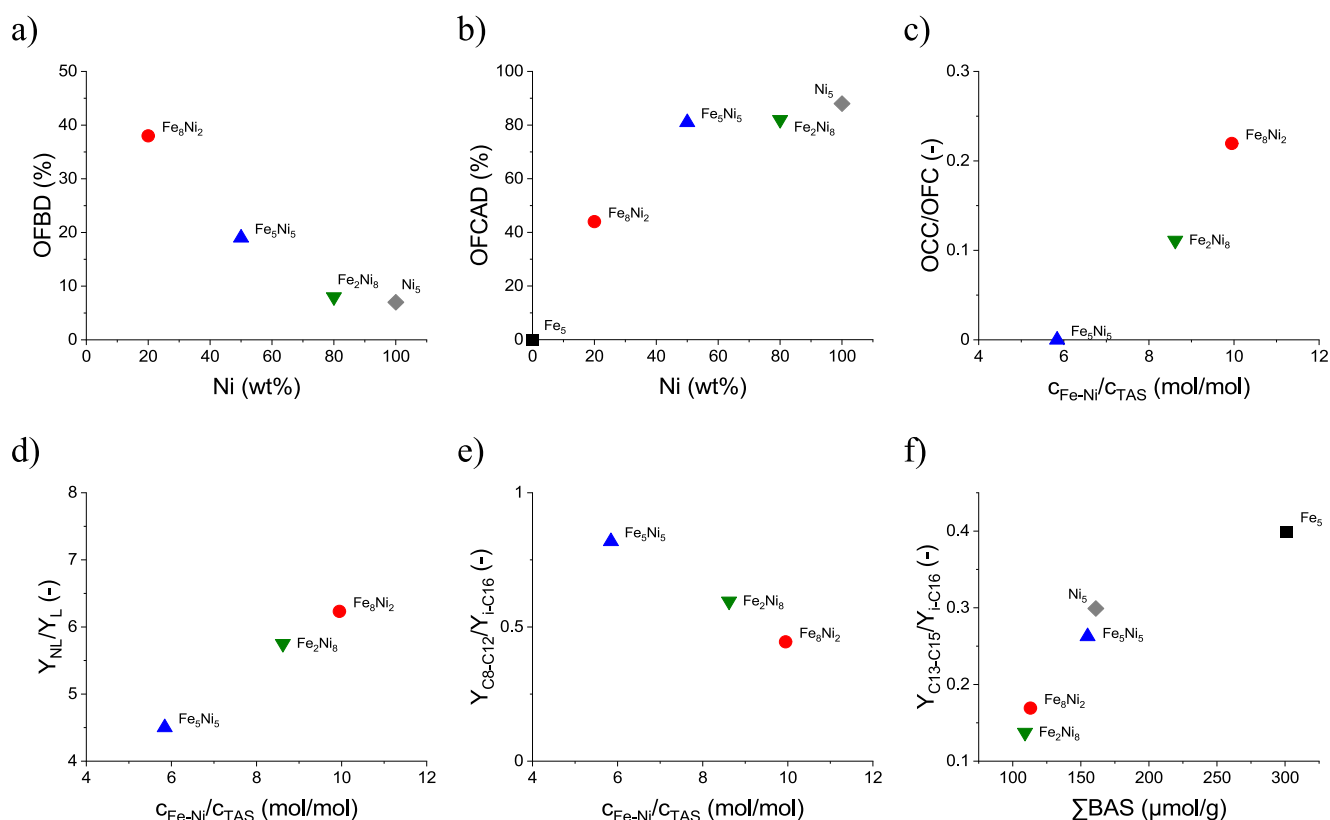


**Fig. 13.** Correlation of the catalytic results with the characterization data: (a) oxygen-free benzene derivatives, (b) oxygen-free cycloalkane derivatives as a function of Ni weight fraction in the catalyst, (c) the ratio of oxygen-containing cyclic compounds and oxygen-free cyclic compounds, (d) the yield ratio of nonlinear (branched and cyclic) and linear products, (e) the yield ratio of jet fuels fraction, C8–C12, and isomerized n-hexadecane, i-C16, as a function of the molar ratio of metals-to-acid site, (f) the yield ratio of long-chain hydrocarbons, C13–C15, and isomerized n-hexadecane, i-C16, as a function of Brønsted acid sites. Conditions: 573 K and 3 MPa of hydrogen with 100 mL of the reaction volume, 0.1 g of catalyst, and the weight ratio of reactant-to-catalyst of 2 and 773 with respect to the isoeugenol and n-hexadecane, respectively, after 4 h. Legend: Fe<sub>5</sub> (black ■), Fe<sub>8</sub>Ni<sub>2</sub> (red ●), Fe<sub>5</sub>Ni<sub>5</sub> (blue ▲), Fe<sub>2</sub>Ni<sub>8</sub> (green ▼), Ni<sub>5</sub> (grey ◆). (For interpretation of the references to colour in this figure legend, the reader is referred to the web version of this article.)

Fe-Ni catalysts was obtained for Fe<sub>5</sub>Ni<sub>5</sub>, which exhibited no strong acid sites and the highest concentration of medium acid sites (Table 2). This is in line with [87] in which Ni-Mo/SAPO-11 with a moderate acidity strength displayed the best performance for producing a jet fuel fraction from long-chain hydrocarbons C15–C18. It should, however, be pointed out that Fe<sub>2</sub>Ni<sub>8</sub> was the most active forwards hydroisomerization of hexadecane giving the highest yield of i-C16 (Table 5). In the case of Fe<sub>5</sub>Ni<sub>5</sub> and Ni<sub>5</sub> catalysts,

increased selectivity to i-C16, and at the same time, decreased selectivity to C8–C12 with increasing conversion indicate catalyst deactivation and suppression of the consecutive pathways. Increased selectivity of isomerized hexadecane with increasing conversion, was also observed for Pt/Beta, Pt/Al<sub>2</sub>O<sub>3</sub>-H-Beta (LL) and Pt/Al<sub>2</sub>O<sub>3</sub>-H-Beta (HL) catalysts with the Pt particle size of 3.1, 2.9 and 2.6 nm, respectively, in the fixed-bed reactor under the same pressure and a lower temperature of 493 K [88]. On the

contrary, decreased selectivity to isomerized hexadecane with increasing conversion, as for  $\text{Fe}_8\text{Ni}_2$ , was obtained in the fixed-bed reactor at 543–583 K for Ni/ZSM-48 exposed to different alkali treatment [71].

Further correlation of the catalytic results with the catalyst characterization data revealed increased activity of benzene ring hydrogenation with an increasing fraction of Ni in the catalyst, leading to formation of cycloalkane derivatives (Fig. 13a,b). This is not surprising considering well known activity of Ni in benzene hydrogenation [89–91]. In the case of the bimetallic catalysts, the ratio of oxygen-containing cyclic compounds and oxygen-free cyclic compounds (OOC/OFC) increased with increasing the metals-to-acid site molar ratio ( $c_{\text{Fe-Ni}}/c_{\text{TAS}}$ ). The same trend was observed for the yield ratio of nonlinear (branched and cyclic) and linear products ( $Y_{\text{NL}}/Y_{\text{L}}$ , Fig. 13d), while for the yield ratio of jet fuel fraction and isomerized n-hexadecane, it was opposite ( $Y_{\text{C8-12}}/Y_{\text{i-C16}}$ , Fig. 13e). In other words, decreasing  $c_{\text{Fe-Ni}}/c_{\text{TAS}}$  led to increased formation of OFC than OCC, more linear products than the branched ones and increased formation of jet fuel fraction than isomerized hexadecane. The yield ratio of long-chain hydrocarbons and isomerized n-hexadecane increased with increased Brønsted acid sites (BAS) for both monometallic and bimetallic catalysts ( $Y_{\text{C13-15}}/Y_{\text{i-C16}}$ , Fig. 13f).

This is in line with [50,51] reporting that stronger acidity leads to more cracking, while mild acidity or BAS promote isomerization. It has been reported in the literature that the mechanism for hydroisomerization-hydrocracking of long-chain alkanes involves in the first step metal sites needed for dehydrogenation of an alkane forming an alkene. This is followed by formation of a carbenium ion on acid sites and subsequent isomerization to an isoolefin [51].

The distribution of all products according to the carbon number (Fig. S10) showed two maxima for all catalysts. As mentioned above, the first maximum was related to methyl-pentadecane, except for the monometallic Fe-catalyst giving dihydroeugenol.

The size of the second maximum, observed at a carbon number of 9 in all other cases, was dependent on the Fe-Ni ratio in the catalyst. The highest second maximum reaching 25 mol% was obtained for  $\text{Fe}_5\text{Ni}_5$ , giving a product mixture containing mainly propyl-cyclohexane and ethyl-methyl-cyclohexane. Lower amounts of product for the second maximum, 12 mol%, were obtained for  $\text{Fe}_8\text{Ni}_2$ , consisting of propyl-phenol, propyl-cyclohexane and butyl-cyclopentane. The second maximum for  $\text{Fe}_2\text{Ni}_8$  and  $\text{Ni}_5$  was related to methyl-octane followed by propyl-cyclohexane, propyl-phenol and dimethyl-heptane.

The distribution of the linear hydrocarbons according to the carbon number (Fig. S11) pointed out on a dominant presence n-tetradecane in the case of  $\text{Fe}_5$  and n-pentadecane for other catalysts. A relatively equal distribution of linear hydrocarbons from C5 to C13 was observed for the monometallic Fe catalyst. For  $\text{Fe}_2\text{Ni}_8$ , the distribution was shifted to the lower linear hydrocarbons with the median at n-heptane, C7. Compared to the latter one, other catalysts showed a lower fraction of C4-C11 and higher for C12-C14 hydrocarbons. Higher amounts of cracked products formed over  $\text{Fe}_2\text{Ni}_8$  are linked with high activity giving 15.5% conversion of hexadecane combined with a consecutive reaction network [51].

## 4. Conclusions

The synergistic effect of Fe and Ni supported on H-Y-5.1 zeolite in the co-processing of n-hexadecane with isoeugenol was investigated in a batch reactor at 573 K and 3 MPa. The results from the catalyst screening experiments clearly showed that both the reaction rate and product distribution strongly depend on the Fe-Ni

metal ratio in the catalysts. The spent catalysts contained ca 40 wt% of coke with predominantly aliphatic species.

In n-hexadecane hydroisomerization-hydrocracking without isoeugenol, the product distribution of C3–C14 exhibited a symmetrical shape, centred at C8, showing preferential cracking of the hexadecane hydrocarbon chain in the centre of the substrate. The presence of just 0.26 wt% isoeugenol made n-hexadecane hydroisomerization-hydrocracking two-fold slower. Lower n-hexadecane conversion compared to the experiment without isoeugenol could be related to strong adsorption of cyclic compounds on the surface of the catalyst and faster isoeugenol hydrodeoxygenation in a diluted system, which points out on the competitive reactions in co-processing.

Correlation of the catalytic results with the characterization data revealed a positive influence of the small medial metal particle size (<6 nm) in the case of n-hexadecane hydroisomerization-hydrocracking. At the same time, the experimental data clearly showed that bifunctionality of the metal-acid catalysts has a key role in the case of hydrodeoxygenation. A low activity towards isoeugenol hydrodeoxygenation was obtained over the monometallic Fe catalyst, while high cracking activity of hexadecane was observed in the presence of Ni. Significantly higher activity of co-processing, compared to other catalysts, was obtained over 2 wt% Fe – 8 wt% Ni/H-Y-5.1 catalysts with the metals particle sizes of 4.6 nm. High activity towards alkylation of n-hexadecane was obtained only for 8 wt% Fe – 2 wt% Ni/H-Y-5.1. Over 5 wt% Fe – 5 wt% Ni/H-Y-5.1 bifunctional catalyst no oxygen-containing cyclic products were detected. This catalyst exhibited the highest hydrogen consumption in temperature programmed desorption, which can serve as a marker for hydrodeoxygenation.

Overall, it can be concluded, that dihydroeugenol conversion, selectivity to nonlinear cracked light hydrocarbons and activity of benzene ring hydrogenation increased with increasing Ni fraction in the iron-nickel catalysts. Except the monometallic Fe catalyst, the isomerized hexadecane was the main product with selectivity of 44–48%. The ratio between nonlinear (branched and cyclic) and linear products was relatively close for all catalysts, with respective amounts 80–86% and 14–20%, respectively.

## Data availability

Data will be made available on request.

## Declaration of Competing Interest

The authors declare that they have no known competing financial interests or personal relationships that could have appeared to influence the work reported in this paper.

## Acknowledgments

The authors are grateful to Business Finland for funding through the project: Catalytic Slurry Hydrotreatment. Samples for electron microscopy were processed and analyzed at the Electron Microscopy Laboratory, Institute of Biomedicine, University of Turku, which receives financial support from Biocenter Finland.

I.S. is grateful for the support from the Ministry of Science and Higher Education of the Russian Federation, under the governmental order for Boreskov Institute of Catalysis (Project No. AAAA-A21-121011390055-8). We acknowledge DESY (Hamburg, Germany), a member of the Helmholtz Association HGF, for the provision of experimental facilities. Parts of this research were carried out at PETRA III and we would like to thank Dr. Edmund Welter for assistance in using beamline P65

## Appendix A. Supplementary material

Supplementary data to this article can be found online at <https://doi.org/10.1016/j.jcat.2023.03.016>.

## References

- [1] A.M. Robinson, J.E. Hensley, J.W. Medlin, Bifunctional catalysts for upgrading of biomass-derived oxygenates: a review, *ACS Catal.* 6 (2016) 5026–5043.
- [2] P. Mäki-Arvela, D.Y. Murzin, Hydrodeoxygenation of lignin-derived phenols: from fundamental studies towards industrial applications, *Catalysts* 7 (2017) 265.
- [3] J. Zakzeski, P.C.A. Bruijninx, A.L. Jongerius, B.M. Weckhuysen, The catalytic valorization of lignin for the production of renewable chemicals, *Chem. Rev.* 110 (2010) 3552–3599.
- [4] M. Saidi, F. Samimi, D. Karimipourfard, T. Nimmanwudipong, B.C. Gates, M.R. Rahimpour, Upgrading of lignin-derived bio-oils by catalytic hydrodeoxygenation, *Energy Environ. Sci.* 7 (2014) 103–129.
- [5] S. Kasakov, H. Shi, D.M. Camaioni, C. Zhao, E. Barath, A. Jentys, J.A. Lercher, Reductive deconstruction of organosolv lignin catalyzed by zeolite supported nickel nanoparticles, *Green Chem.* 17 (2015) 5079–5090.
- [6] P. Bajpai, Pretreatment of Lignocellulosic Biomass for Biofuel Production, Springer Singapore, Singapore, 2016.
- [7] S.N. Sun, S.L. Sun, X.F. Cao, R.C. Sun, The role of pretreatment in improving the enzymatic hydrolysis of lignocellulosic materials, *Bioresour. Technol.* 199 (2016) 49–58.
- [8] J. Ralph, K. Lundquist, G.S. Brunow, F. Lu, H. Kim, P.F. Schatz, J.M. Marita, R.D. Hatfield, S.A. Ralph, J.H. Christensen, W. Boerjan, Lignins: natural polymers from oxidative coupling of 4-hydroxyphenyl-propanoids, *Phytochem. Rev.*, 3 (2004) 26–60.
- [9] A. Aho, N. Kumar, A.V. Lashkul, K. Eränen, M. Ziolek, P. Decyk, T. Salmi, B. Holmbom, M. Hupa, D.Y. Murzin, Catalytic upgrading of woody biomass derived pyrolysis vapours over iron modified zeolites in a dual-fluidized bed reactor, *Fuel* 89 (2010) 1992–2000.
- [10] A.V. Bridgwater, Review of fast pyrolysis of biomass and product upgrading, *Biomass Bioenergy* 38 (2012) 68–94.
- [11] M. Sharifzadeh, M. Sadeqzadeh, M. Guo, T.N. Borhani, N. Konda, M.C. Garcia, L. Wang, J. Hallett, N. Shah, The multi-scale challenges of biomass fast pyrolysis and bio-oil upgrading: review of the state of art and future research directions, *Prog. Energy Combust. Sci.* 71 (2019) 1–80.
- [12] C. Lindfors, P. Mäki-Arvela, P. Paturi, A. Aho, K. Eränen, J. Hemming, M. Peurla, D. Kubička, I.L. Simakova, D.Y. Murzin, Hydrodeoxygenation of isoeugenol over Ni- and co-supported catalysts, *ACS Sustain. Chem. Eng.* 7 (2019) 14545–14560.
- [13] F.L. Mendes, V.T. da Silva, M.E. Pacheco, F.S. Toniolo, C.A. Henriques, Bio-oil hydrotreating using nickel phosphides supported on carbon-covered alumina, *Fuel* 241 (2019) 686–694.
- [14] P.M. Mortensen, D. Gardini, H.W.P. de Carvalho, C.D. Damsgaard, J.D. Grunwaldt, P.A. Jensen, J.B. Wagner, A.D. Jensen, Stability and resistance of nickel catalysts for hydrodeoxygenation: carbon deposition and effects of sulfur, potassium, and chlorine in the feed, *Catal. Sci. Technol.* 4 (2014) 3672–3686.
- [15] A.E. Coumans, E.J.M. Hensen, A real support effect on the hydrodeoxygenation of methyl oleate by sulfided NiMo catalysts, *Catal. Today* 298 (2017) 181–189.
- [16] M. Anand, A.K. Sinha, Temperature-dependent reaction pathways for the anomalous hydrocracking of triglycerides in the presence of sulfided Co-Mo-catalyst, *Bioresour. Technol.* 126 (2012) 148–155.
- [17] A. Demirbas, Competitive liquid biofuels from biomass, *Appl. Energy* 88 (2011) 17–28.
- [18] L. Hu, X.Y. Wei, Y.H. Kang, X.H. Guo, M.L. Xu, Z.M. Zong, Mordenite-supported ruthenium catalyst for selective hydrodeoxygenation of lignin model compounds and lignin-derived bio-oil to produce cycloalkanes, *J. Energy Inst.* 96 (2021) 269–279.
- [19] H.W. Lee, B.R. Jun, H. Kim, D.H. Kim, J.K. Jeon, S.H. Park, C.H. Ko, T.W. Kim, Y.K. Park, Catalytic hydrodeoxygenation of 2-methoxy phenol and dibenzofuran over Pt/mesoporous zeolites, *Energy* 81 (2015) 33–40.
- [20] N.K.G. Silva, R.A.R. Ferreira, R.M. Ribas, R.S. Monteiro, M.A.S. Barrozo, R.R. Soares, Gas-phase hydrodeoxygenation (HDO) of guaiacol over Pt/Al<sub>2</sub>O<sub>3</sub> catalyst promoted by Nb<sub>2</sub>O<sub>5</sub>, *Fuel* 287 (2021).
- [21] I.T. Ghampson, C. Sepilveda, R. Garcia, J.L.G. Fierro, N. Escalona, Carbon nanofiber-supported reo<sub>x</sub> catalysts for the hydrodeoxygenation of lignin-derived compounds, *Catal. Sci. Technol.* 6 (2016) 4356–4369.
- [22] X.H. Zhang, W.W. Tang, Q. Zhang, T.J. Wang, L.L. Ma, Hydrocarbons Production from Lignin-Derived Phenolic Compounds over Ni/SiO<sub>2</sub> Catalyst, 8th International Conference on Applied Energy (ICAE2016), 105 (2017) 518–523.
- [23] D.N. Gao, Y. Xiao, A. Varma, Guaiacol hydrodeoxygenation over platinum catalyst: reaction pathways and kinetics, *Ind. Eng. Chem. Res.* 54 (2015) 10638–10644.
- [24] C.A. Teles, R.C. Rabelo-Neto, G. Jacobs, B.H. Davis, D.E. Resasco, F.B. Noronha, Hydrodeoxygenation of phenol over zirconia-supported catalysts: the effect of metal type on reaction mechanism and catalyst deactivation, *ChemCatChem* 9 (2017) 2850–2863.
- [25] P.M. Mortensen, J.D. Grunwaldt, P.A. Jensen, A. Degn Jensen, Screening of catalysts for hydrodeoxygenation of phenol as a model compound for bio-oil, *ACS Catal.* 3 (2013) 1774–1785.
- [26] S. Tieuli, P. Mäki-Arvela, M. Peurla, K. Eränen, J. Warna, G. Cruciani, F. Menegazzo, D.Y. Murzin, M. Signoretto, Hydrodeoxygenation of isoeugenol over Ni-SBA-15: kinetics and modelling, *Appl. Catal. A-Gen.* 580 (2019) 1–10.
- [27] C.J. Chen, A. Bhan, Mo<sub>2</sub>C modification by CO<sub>2</sub>, H<sub>2</sub>O, and O<sub>2</sub>: effects of oxygen content and oxygen source on rates and selectivity of m-cresol hydrodeoxygenation, *ACS Catal.* 7 (2017) 1113–1122.
- [28] P.M. de Souza, R.C. Rabelo-Neto, L.E.P. Borges, G. Jacobs, B.H. Davis, U.M. Graham, D.E. Resasco, F.B. Noronha, Effect of zirconia morphology on hydrodeoxygenation of phenol over Pd/ZrO<sub>2</sub>, *ACS Catal.* 5 (2015) 7385–7398.
- [29] C. Gonzalez, P. Marin, F.V. Diez, S. Ordonez, Gas-phase hydrodeoxygenation of benzaldehyde, benzyl alcohol, phenyl acetate, and anisole over precious metal catalysts, *Ind. Eng. Chem. Res.* 55 (2016) 2319–2327.
- [30] L. He, Y. Qin, H. Lou, P. Chen, Highly dispersed molybdenum carbide nanoparticles supported on activated carbon as an efficient catalyst for the hydrodeoxygenation of vanillin, *RSC Adv.* 5 (2015) 43141–43147.
- [31] J.L. Santos, M. Alda-Onggar, V. Fedorov, M. Peurla, K. Eränen, P. Mäki-Arvela, M. A. Centeno, D.Y. Murzin, Hydrodeoxygenation of vanillin over carbon supported metal catalysts, *Appl. Catal. A-Gen.* 561 (2018) 137–149.
- [32] M.Y. Zhang, Y.L. Hu, H.Y. Wang, H.Y. Li, X. Han, Y.M. Zeng, C.C. Xu, A Review of bio-oil upgrading by catalytic hydrotreatment: advances, challenges, and prospects, *Mol. Catal.* 504 (2021) 20.
- [33] C. Zhang, J. Xing, L. Song, H.C. Xin, S. Lin, L.S. Xing, X.B. Li, Aqueous-phase hydrodeoxygenation of lignin monomer eugenol: influence of Si/Al ratio of HZSM-5 on catalytic performances, *Catal. Today* 234 (2014) 145–152.
- [34] J.B. Qi, X.Y. Sung, S.F. Tang, Y.Y. Sun, C. Xu, X.Y. Li, X.B. Li, Integrated study on the role of solvent, catalyst and reactant in the hydrodeoxygenation of eugenol over nickel-based catalysts, *Appl. Catal. A-Gen.* 535 (2017) 24–31.
- [35] T. Nimmanwudipong, R.C. Runnebaum, S.E. Ebeler, D.E. Block, B.C. Gates, Upgrading of lignin-derived compounds: reactions of eugenol catalyzed by HY zeolite and by Pt/gamma-Al<sub>2</sub>O<sub>3</sub>, *Catal. Lett.* 142 (2012) 151–160.
- [36] X.P. Li, L. Chen, G.Y. Chen, J.G. Zhang, J.P. Liu, The relationship between acidity, dispersion of nickel, and performance of Ni/Al-SBA-15 catalyst on eugenol hydrodeoxygenation, *Renew. Energy* 149 (2020) 609–616.
- [37] A. Bjelic, M. Grilc, B. Likozar, Bifunctional metallic-acidic mechanisms of hydrodeoxygenation of eugenol as lignin model compound over supported Cu, Ni, Pd, Pt, Rh and Ru catalyst materials, *Chem. Eng. J.* 394 (2020) 14.
- [38] L. Bomont, M. Alda-Onggar, V. Fedorov, A. Aho, J. Peltonen, K. Eränen, M. Peurla, N. Kumar, J. Wärna, V. Russo, P. Mäki-Arvela, H. Grenman, M. Lindblad, D.Y. Murzin, Production of cycloalkanes in hydrodeoxygenation of isoeugenol over Pt- and Ir-modified bifunctional catalysts, *Eur. J. Inorg. Chem.* 2841–2854 (2018).
- [39] M. Alda-Onggar, Hydrodeoxygenation of Bio-Oil Model Compounds using Alumina, Zirconia and Carbon Supported Metal Catalysts, Laboratory of Industrial Chemistry and Reaction Engineering, Åbo Akademi University, Finland, 2018.
- [40] M. Alda-Onggar, P. Mäki-Arvela, K. Eränen, A. Aho, J. Hemming, P. Paturi, M. Peurla, M. Lindblad, I.L. Simakova, D.Y. Murzin, Hydrodeoxygenation of isoeugenol over alumina-supported Ir, Pt, and Re catalysts, *ACS Sust. Chem. Eng.* 6 (2018) 16205–16218.
- [41] E. Commission, Directive (EU) 2018/2001 of the European Parliament and of the Council of 11 December 2018 on the Promotion of the Use of Energy from Renewable Sources (recast), *Off. J. Eur. Union.* L328 2018, pp. 82 – 209.
- [42] S. Bezergianni, A. Dimitriadis, D. Karonis, Diesel decarbonization via effective catalytic co-hydroprocessing of residual lipids with gas-oil, *Fuel* 136 (2014) 366–373.
- [43] S. Bezergianni, A. Dimitriadis, O. Kikhtyanin, D. Kubička, Refinery co-processing of renewable feeds, *Prog. Energy Combust. Sci.* 68 (2018) 29–64.
- [44] A. Corma, G.W. Huber, L. Sauvanaud, P. O'Connor, Processing biomass-derived oxygenates in the oil refinery: catalytic cracking (FCC) reaction pathways and role of catalyst, *J. Catal.* 247 (2007) 307–327.
- [45] R. Pujro, M. Panero, M. Bertero, U. Sedran, M. Falco, Hydrogen transfer between hydrocarbons and oxygenated compounds in coprocessing bio-oils in fluid catalytic cracking, *Energy Fuels* 33 (2019) 6473–6482.
- [46] A. Pinheiro, D. Hudebine, N. Dupassieux, C. Geantet, Impact of oxygenated compounds from lignocellulosic biomass pyrolysis oils on gas oil hydrotreatment, *Energy Fuels* 23 (2009) 1007–1014.
- [47] F.D. Mercader, M.J. Groeneveld, S.R.A. Kersten, C. Geantet, G. Toussaint, N.W.J. Way, C.J. Schaverien, K.J.A. Hogendoorn, Hydrodeoxygenation of pyrolysis oil fractions: process understanding and quality assessment through co-processing in refinery units, *Energy Environ. Sci.* 4 (2011) 985–997.
- [48] A.E. Atabani, A.S. Silitonga, H.C. Ong, T.M.I. Mahlia, H.H. Masjuki, I.A. Badruddin, H. Fayaz, Non-edible vegetable oils: a critical evaluation of oil extraction, fatty acid compositions, biodiesel production, characteristics, engine performance and emissions production, *Renew. Sust. Energy Rev.* 18 (2013) 211–245.
- [49] R.R. Ding, Y.L. Wu, Y. Chen, J.M. Liang, J. Liu, M.D. Yang, Effective hydrodeoxygenation of palmitic acid to diesel-like hydrocarbons over MoO<sub>2</sub>/CNTs catalyst, *Chem. Eng. Sci.* 135 (2015) 517–525.
- [50] T.K. Khel, P. Mäki-Arvela, M. Azkaar, Z. Vajglová, A. Aho, J. Hemming, M. Peurla, K. Eränen, N. Kumar, D.Y. Murzin, Hexadecane hydrocracking for production of jet fuels from renewable diesel over proton and metal modified H-beta zeolites, *Mol. Catal.* 476 (2019).

- [51] P. Mäki-Arvela, T.K. Khel, M. Azkaar, S. Engblom, D.Y. Murzin, Catalytic hydroisomerization of long-chain hydrocarbons for the production of fuels, *Catalysts* 8 (2018) 534.
- [52] M. Azkaar, Z. Vajglóvá, P. Mäki-Arvela, A. Aho, N. Kumar, H. Palonen, K. Eranen, M. Peurla, L.A. Kullikov, A.L. Maximov, C. Mondelli, J. Perez-Ramirez, D.Y. Murzin, Hydrocracking of hexadecane to jet fuel components over hierarchical Ru-modified Faujasite zeolite, *Fuel* 278 (2020) 13.
- [53] A. Pimerzin, A. Savinov, A. Vutolkina, A. Makova, A. Glotov, V. Vinokurov, Transition metal sulfides- and noble metal-based catalysts for N-hexadecane hydroisomerization: a study of poisons tolerance, *Catalysts* 10 (2020) 594.
- [54] M. Zhang, Y.J. Chen, L. Wang, Q.M. Zhang, C.W. Tsang, C.H. Liang, Shape selectivity in hydroisomerization of hexadecane over pt supported on 10-ring zeolites: ZSM-22, ZSM-23, ZSM-35, and ZSM-48, *Ind. Eng. Chem. Res.* 55 (2016) 6069–6078.
- [55] M.E. Martínez-Klimov, P. Mäki-Arvela, Z. Vajglóvá, M. Alda-Onggar, I. Angervo, N. Kumar, K. Eränen, M. Peurla, M.H. Calimli, J. Muller, A. Shchukarev, I.L. Simakova, D.Y. Murzin, Hydrodeoxygenation of isoeugenol over carbon-supported Pt and Pt-Re catalysts for production of renewable jet fuel, *Energy Fuels* 35 (2021) 17755–17768.
- [56] W.N.A.W. Khalit, T.S. Marliza, N. Asikin-Mijan, M.S. Gamal, M.I. Saiman, M.L. Ibrahim, Y.H. Taufiq-Yap, Development of bimetallic nickel-based catalysts supported on activated carbon for green fuel production, *RSC Adv.* 10 (2020) 37218–37232.
- [57] M. Al-Muttaqii, F. Kurniawansyah, D.H. Prajitno, A. Roesyadi, Hydrocracking of coconut oil over Ni-Fe/HZSM-5 catalyst to produce hydrocarbon biofuel, *Indones. J. Chem.* 19 (2019) 319–327.
- [58] N. Gorocs, D. Mudri, J. Matyasi, J. Balla, The determination of GC-MS relative molar responses of some n-alkanes and their halogenated analogs, *J. Chromatogr. Sci.* 51 (2013) 138–145.
- [59] M.C. Wright, R.W. Court, F.C.A. Kafantaris, F. Spathopoulos, M.A. Sephton, A new rapid method for shale oil and shale gas assessment, *Fuel* 153 (2015) 231–239.
- [60] M.J. Wulfers, F.C. Jentoft, Identification of carbonaceous deposits formed on H-mordenite during alkane isomerization, *J. Catal.* 307 (2013) 204–213.
- [61] M. Diaz, J. Valecillos, S. Izaddoust, A.T. Aguayo, J. Bilbao, Coke deactivation and regeneration of HZSM-5 zeolite catalysts in the oligomerization of 1-butene, *Appl. Catal. B-Env.* 291 (2021).
- [62] J. Valecillos, E. Epelde, J. Albo, A.T. Aguayo, J. Bilbao, P. Castaño, Slowing down the deactivation of H-ZSM-5 Zeolite catalyst in the methanol-to-olefin (MTO) reaction by P or Zn modifications, *Catal. Today* 348 (2020) 243–256.
- [63] M. Guisnet, P. Magnoux, Organic chemistry of coke formation, *Appl. Catal. A-Gen.* 212 (2001) 83–96.
- [64] A. Holmen, O.A. Lindvag, Coke formation on nickel-chromium-iron alloys, *J. Mater. Sci.* 22 (1987) 4518–4522.
- [65] E. Pippel, J. Woltersdorf, H.J. Grabke, Microprocesses of metal dusting on iron-nickel alloys and their dependence on the alloy composition, *Mater. Corros.-Werkstoffe und Korrosion* 54 (2003) 747–751.
- [66] E. Pippel, J. Woltersdorf, R. Schneider, Micromechanisms of metal dusting on Fe-base and Ni-base alloys, *Mater. Corros.-Werkstoffe und Korrosion* 49 (1998) 309–316.
- [67] O.A. Sahraei, A. Desgagnes, F. Larachi, M.C. Iliuta, Ni-Fe catalyst derived from mixed oxides Fe/Mg-bearing metallurgical waste for hydrogen production by steam reforming of biodiesel by-product: investigation of catalyst synthesis parameters and temperature dependency of the reaction network, *Appl. Catal. B-Env.* 279 (2020).
- [68] M. Haouas, F. Taulelle, C.h. Martineau, Recent advances in application of <sup>27</sup>Al NMR spectroscopy to materials science, *Prog. Nucl. Magn. Reson. Spectrosc.* 94–95 (2016) 11–36.
- [69] Y.J. Chen, C. Li, X. Chen, Y. Liu, C.H. Liang, Synthesis of ZSM-23 zeolite with dual structure directing agents for hydroisomerization of n-hexadecane, *Micropor. Mesopor. Mat.* 268 (2018) 216–224.
- [70] P. Lanzafoame, S. Perathoner, G. Centi, E. Heracleous, E.F. Iliopoulou, K.S. Triantafyllidis, A.A. Lappas, Effect of the structure and mesoporosity in Ni/Zeolite catalysts for n-hexadecane hydroisomerisation and hydrocracking, *ChemCatChem* 9 (2017) 1632–1640.
- [71] M. Zhang, C. Li, X. Chen, Y.J. Chen, C.H. Liang, Hierarchical ZSM-48-supported nickel catalysts with enhanced hydroisomerization performance of hexadecane, *Ind. Eng. Chem. Res.* 58 (2019) 19855–19861.
- [72] R.A. Keogh, D. Sparks, J.L. Hu, I. Wender, J.W. Tierney, W. Wang, B.H. Davis, Hydroisomerization and hydrocracking of n-hexadecane over a platinum-promoted sulfated zirconia catalyst, *Energy Fuels* 8 (1994) 755–762.
- [73] R. Kenmogne, A. Finiels, C. Cammarano, V. Hulea, F. Fajula, Hydroconversion of n-hexadecane over bifunctional microporous and mesoporous model catalysts. influence of pore architecture on selectivity, *J. Catal.* 329 (2015) 348–354.
- [74] K.P. de Jong, J. Zecevic, H. Friedrich, P.E. de Jongh, M. Bulut, S. van Donk, R. Kenmogne, A. Finiels, V. Hulea, F. Fajula, Zeolite Y crystals with trimodal porosity as ideal hydrocracking catalysts, *Angew. Chem. Int. Ed.* 49 (2010) 10074–10078.
- [75] X.J. Dai, Y. Cheng, M. Si, Q. Wei, L.Y. Zhao, X.H. Wang, W.B. Huang, H.R. Liu, Y.S. Zhou, Synthesis of nickel in situ modified SAPO-11 molecular sieves and hydroisomerization performance of their NiWS supported catalysts, *Front. Chem.* 9 (2021).
- [76] N. Pfriem, P.H. Hintermeier, S. Eckstein, S. Kim, Q. Liu, H. Shi, L. Milakovic, Y. Liu, G.L. Haller, E. Barath, Y. Liu, J.A. Lercher, Role of the ionic environment in enhancing the activity of reacting molecules in zeolite pores, *Science* 372 (2021) 952–957.
- [77] P.H. Yan, M.M.J. Li, E. Kennedy, A. Adesina, G.Y. Zhao, A. Setiawan, M. Stockenhuber, The role of acid and metal sites in hydrodeoxygenation of guaiacol over Ni/beta catalysts, *Catal. Sci. Technol.* 10 (2020) 810–825.
- [78] K.B. Baharudin, M. Arumugam, J. Hunns, A.F. Lee, E. Mayes, Y.H. Taufiq-Yap, K. Wilson, D. Derawi, Octanoic acid hydrodeoxygenation over bifunctional Ni/Al-SBA-15 catalysts, *Catal. Sci. Technol.* 9 (2019) 6673–6680.
- [79] H. Shafaghath, P.S. Rezaei, W. Daud, Catalytic hydrodeoxygenation of simulated phenolic bio-oil to cycloalkanes and aromatic hydrocarbons over bifunctional metal/acid catalysts of Ni/HBeta, Fe/HBeta and NiFe/HBeta, *J. Ind. Eng. Chem.* 35 (2016) 268–276.
- [80] T. Prasamsri, M. Shetty, K. Murugappan, Y. Roman-Leshkov, Insights into the catalytic activity and surface modification of mo<sub>03</sub> during the hydrodeoxygenation of lignin-derived model compounds into aromatic hydrocarbons under low hydrogen pressures, *Energy Env. Sci.* 7 (2014) 2660–2669.
- [81] W.S. Lee, Z.S. Wang, R.J. Wu, A. Bhan, Selective vapor-phase hydrodeoxygenation of anisole to benzene on molybdenum carbide catalysts, *J. Catal.* 319 (2014) 44–53.
- [82] K. Xie, S.Z. Wang, P. Li, X.J. Li, Z.Y. Yang, X.Y. An, C.C. Guo, Z. Tan, Synthesis of tetralin and chromane derivatives via in-catalyzed intramolecular hydroarylation, *Tetrahedron Lett.* 51 (2010) 4466–4469.
- [83] T. Okuhara, T. Nakajo, Process for Producing Aromatic Compounds by Friedel-Crafts Reaction, US Patent, US711578B2, 2003.
- [84] J.M. Begouin, F. Capitta, X. Wu, M. Niggemann, Diastereoselective synthesis of indanes and tetralins via intramolecular friedel-crafts reaction, *Organic Lett.* 15 (2013) 1370–1373.
- [85] Z. Maeno, H. Torii, S. Yamada, T. Mitsudome, T. Mizugaki, K. Jitsukawa, Synthesis of tetraline derivatives through depolymerization of polyethers with aromatic compounds using a heterogeneous titanium-exchanged montmorillonite catalyst, *RSC Adv.* 6 (2016) 89231–89233.
- [86] S.G. Zhang, Y.L. Zhang, J.W. Tierney, I. Wender, Anion-modified zirconia: effect of metal promotion and hydrogen reduction on hydroisomerization of n-hexadecane and fischer-tropsch waxes, *Fuel Process. Technol.* 69 (2001) 59–71.
- [87] G.H. King, S.Y. Liu, Q.X. Guan, W. Li, Investigation on hydroisomerization and hydrocracking of C15–C18 n-alkanes utilizing a hollow tubular Ni-Mo/SAPO-11 catalyst with high selectivity of jet fuel, *Catal. Today* 330 (2019) 109–116.
- [88] N. Batalha, S. Morisset, L. Pinard, I. Maupin, J.L. Lemberon, F. Lemos, Y. Pouilloux, BEA zeolite nanocrystals dispersed over alumina for n-hexadecane hydroisomerization, *Micropor. Mesopor. Mat.* 166 (2013) 161–166.
- [89] D.Y. Murzin, N.A. Sokolova, N.V. Kulkova, M.I. Temkin, Kinetics of liquid-phase hydrogenation of benzene and toluene on a nickel-catalyst, *Kinet. Catal.* 30 (1989) 1176–1181.
- [90] P.G. Savva, K. Goundani, J. Vakros, K. Bourikas, C. Fountzoula, D. Vattis, A. Lycourghiotis, C. Kordulis, Benzene Hydrogenation over Ni/Al<sub>2</sub>O<sub>3</sub> catalysts prepared by conventional and sol-gel techniques, *Appl. Catal. B-Env.* 79 (2008) 199–207.
- [91] L. Daza, B. Pawelec, J.A. Anderson, J.L.G. Fierro, Relationship between reduced nickel and activity for benzene hydrogenation on Ni-USY zeolite catalysts, *Appl. Catal. A-Gen.* 87 (1992) 145–156.